

The interannual variability of potential temperature in the central Labrador Sea

Hao Luo,¹ Annalisa Bracco,¹ Igor Yashayaev,² and Emanuele Di Lorenzo¹

Received 17 February 2012; revised 11 September 2012; accepted 12 September 2012; published 19 October 2012.

[1] The interannual variability of potential temperature in the central Labrador Sea is studied with a suite of numerical simulations with an eddy-resolving regional ocean model and compared with available observations. The model successfully reproduces the observed variations in potential temperature at depths comprised between 150 and 2000 m over the period 1980–2009, capturing also the warming trend of the last decade and the deep water formation event in 2008. The suite of experiments allows for quantifying the contribution from the physical forcings responsible for the interannual variability of potential temperature in the region. The local atmospheric forcing drives the interannual signal by driving convection, while the incoming current system along the east coast of Greenland is responsible for about half of the warming trend ($\sim 0.3\text{--}0.4^\circ\text{C}$) during the last decade through restratification process. The lateral transport of Irminger water in the convective region into the central Labrador Sea is further analyzed integrating a passive tracer. It is found that the overall amount of Irminger water transported in the convective region of the Labrador Sea is directly correlated with the amount of vertical convective mixing. In the last decade, following the decrease in convective activity, the model reveals a substantial decrease in concentration of Irminger Current water below 500 m in the Labrador Sea interior: by 2010 the overall amount is less than half than in the previous 20 years.

Citation: Luo, H., A. Bracco, I. Yashayaev, and E. Di Lorenzo (2012), The interannual variability of potential temperature in the central Labrador Sea, *J. Geophys. Res.*, 117, C10016, doi:10.1029/2012JC007988.

1. Introduction

[2] The Labrador Sea is one of the few sites in the world ocean where deep convection occurs. In this region the oceanic winter heat loss due to intense atmosphere-ocean interactions results in convective mixing both in its interior [Marshall and Schott, 1999] and over its shelves [Pickart *et al.*, 2002].

[3] Along the shelf, the East Greenland Current (EGC) enters the Labrador Sea at the surface carrying cold and fresh Arctic waters around Greenland, where it changes name to West Greenland Current (WGC) and then Labrador Current (LC) while flowing around the basin. Immediately off the shelf the warm and salty subsurface Irminger Current (IC) flows firmly attached to the sloping bottom. As noted by Fratantoni and Pickart [2007], the Greenland and Irminger Currents may be thought of as one current system, merged in velocity structure, but with distinct water masses. In the

center of the basin, convective events mix the surface waters to depths occasionally exceeding 2000 m [Lazier, 1980; Clarke and Gascard, 1983; Gascard and Clarke, 1983; Lazier *et al.*, 2002; Yashayaev, 2007; Yashayaev *et al.*, 2003, 2007a] and form a dense water mass, the Labrador Sea Water (LSW), that spreads across the northwest Atlantic between 1000 and 2200 m [Talley and McCartney, 1982]. Below the LSW, the water column is occupied by denser, convective waters, or overflow waters, originating from outside the Labrador Sea: the Northeast Atlantic Deep Water (NEADW) and the Denmark Strait Overflow Water (DSOW). Together with the deep overflow waters from the Nordic Seas, the LSW contributes to the North Atlantic Deep Water (NADW) and to the Atlantic branch of the Meridional Overturning Circulation (AMOC). Therefore, understanding what drives the interannual variability in the Labrador Sea has far-reaching impacts in the study of the AMOC and the global climate system.

[4] Although deep convection in this region is predominantly driven by variations in local surface buoyancy forcing, recent work has shown that mesoscale eddies play an important role in the lateral heat exchange across the basin and contribute to its restratification [Lazier *et al.*, 2002; Lilly *et al.*, 2003; Straneo, 2006a, 2006b; Khatiwala and Visbeck, 2000; Hátún *et al.*, 2007; Avsic *et al.*, 2006]. In a steady state, buoyancy from the boundary current system must be drawn inward to balance the extreme wintertime cooling and evaporation. Since the interior Labrador Sea is

¹School of Earth and Atmospheric Sciences, Georgia Institute of Technology, Atlanta, Georgia, USA.

²Fisheries and Oceans Canada, Bedford Institute of Oceanography, Dartmouth, Nova Scotia, Canada.

Corresponding author: H. Luo, School of Earth and Atmospheric Sciences, Georgia Institute of Technology, 311 Ferst Dr., Atlanta, GA 30332, USA. (hao.luo@eas.gatech.edu)

©2012. American Geophysical Union. All Rights Reserved.
0148-0227/12/2012JC007988

essentially a region of closed mean streamlines [Lavender *et al.*, 2002], oceanic buoyancy transport is believed to be accomplished by eddy fluxes extracting buoyancy from the boundary current system.

[5] Labrador Sea eddies have been grouped into three categories based on their formation mechanism: Irminger Rings (IRs), boundary current eddies (BCEs) and convective eddies (CEs). Originated from the warm boundary current, the IRs have been identified by numerical modeling [Eden and Böning, 2002; Katsman *et al.*, 2004; Bracco *et al.*, 2008; Gelderloos *et al.*, 2011] and observational studies [Lilly *et al.*, 2003; Hátún *et al.*, 2007; Rykova *et al.*, 2009] as fundamental contributors to the lateral transfer of heat and salt from the Irminger Current along the coast of Greenland to the interior of the basin, where deep convection occurs. The analysis by Lilly *et al.* [2003] and Rykova *et al.* [2009] suggests also that at least since 1997 some IRs have been able to survive the winter heat loss maintaining their identity while being convectively modified at their interior. Long-lived (up to 2 years), they have a diameter of 40–50 km and are formed by topographically localized baroclinic instability at about 61–62°N [Bracco and Pedlosky, 2003; Luo *et al.*, 2011]. IRs represent the major source of eddy kinetic energy (EKE) in the basin. The BCEs are generated by baroclinic instability of the boundary current system [Spall, 2004], and the fluxes associated with them may be simply parameterized in terms of the isopycnal gradient between the interior and the boundary current [Straneo, 2006a, 2006b]. They are about three times smaller than Irminger Rings and their diameter is of the same order of magnitude as the local Rossby radius of deformation [Eden and Böning, 2002; Chanut *et al.*, 2008]. Finally, CEs are generated by baroclinic instability in the convective patch, as demonstrated by numerical studies of open ocean deep convection [Jones and Marshall, 1997; Marshall and Schott, 1999].

[6] Hydrographic observations have shown that the sub-polar North Atlantic Ocean recently experienced significant changes on the interannual and decadal time scales including freshening [Dickson *et al.*, 2002, 2003; Bersch, 2002], and weakening of the circulation [Häkkinen and Rhines, 2004; Lohmann *et al.*, 2009]. These variations may be driven by changes in local atmospheric fluxes that in turn are correlated with the North Atlantic Oscillation (NAO) [Dickson *et al.*, 1996; Visbeck *et al.*, 2003; Yashayaev, 2007; Lohmann *et al.*, 2009], but may also be influenced by variability in the lateral mixing exerted by mesoscale eddies [Khatiwala and Visbeck, 2000; Avsic *et al.*, 2006].

[7] In the Labrador Sea, over the last three decades, deep convection was most intense during the late 1980s and early 1990s, and weakened since 1995, in conjunction with a general warming of the basin [Lazier *et al.*, 2002; Yashayaev *et al.*, 2003; van Aken *et al.*, 2011]. Several studies investigated the sources of such variability. Marshall and Schott [1999] have shown that deep convection in the Labrador Sea strongly depends on the properties of the incoming boundary current system. Häkkinen and Rhines [2004] and Holland *et al.* [2008] suggest that the reduction of deep convection and the increase of potential temperature (PT) in the Labrador Sea during the second half of the 1990s is linked to a general weakening of the North Atlantic subpolar gyre circulation. Myers *et al.* [2007] find that the formation of LSW is highly correlated with the Irminger Seawater

transport at Cape Farewell with a lag of 1 year. Marsh *et al.* [2008] suggest that the hydrographic variations in the Labrador Sea are related to the anomalous convergence of ocean heat transport associated with fluctuations in the subpolar gyre. Böning *et al.* [2006] show with a high-resolution ocean circulation model that the weakening in the strength of the boundary current system in the Labrador Sea during the 1990s is directly correlated to the strength of the subpolar gyre and argue that this is driven by changes in the atmospheric fluxes described by the NAO. This is confirmed by the analysis of Labrador Current transport anomalies from 1993 to 2004 using satellite and conductivity-temperature-depth (CTD) data by Han *et al.* [2010]. This work, however, notices a rebound of the transport in the 2000s and no clear trends. Furthermore, using current meter observations, Schott *et al.* [2004] and Fischer *et al.* [2010] have found no evidence of weakening in the NADW outflow during 1993 to 2001. Similarly, moored current meter records at 53°N do not display any detectable decadal trend in the strength of the deep and near-bottom flow out of the Labrador Sea [Fischer *et al.*, 2010], confirming the analysis of the mean boundary current transport in the Labrador Sea during the 1992–2007 period using Simple Ocean Data Assimilation (SODA) reanalysis [Schott *et al.*, 2009]. SODA, on the other hand, is unable to reproduce the mean state and interannual variability of potential temperature in the Labrador Basin (e.g., Figures 3 and 4 in section 4.2) due to a poor representation of water properties below 1000 m [Carton and Giese, 2008].

[8] Understanding the physical mechanisms driving the interannual variability of PT in the Labrador Sea is important also in light of the changes in heat fluxes and transport that the North Atlantic may experience under climate change. This variability may be driven by changes in water properties from the incoming boundary current, by changes in the local wind stress and heat fluxes, possibly linked to the NAO or the Arctic Oscillation (AO) [Thompson and Wallace, 1998], or by an interplay of both.

[9] In this paper, we use a regional ocean model to explore the role of those potential contributors. Modeling the Labrador Sea variability is challenging, due to the high resolution required to resolving the Rossby deformation radius, which is about 13 km, and the eddy field in the basin, and to uncertainties in the reanalysis product for heat and momentum fluxes at high latitudes. We adopt the Regional Ocean Modeling System (ROMS) in a configuration previously implemented to investigate the control mechanisms of the interannual variability of the surface EKE in the Labrador Sea [Luo *et al.*, 2011, hereafter referred to as LBD11]. LBD11 have shown that this configuration is capable of capturing well the mean circulation and the eddy activity in the basin when compared with available observations, while allowing for long enough integrations and sensitivity studies to investigate the sources of interannual variability in the basin. Here we show that with adequate resolution it is possible to reproduce the observed variability in PT throughout the water column accurately.

2. Model and Data

2.1. Model Configuration

[10] In this study we use the Regional Ocean Modeling System (ROMS) [Shechepetkin and McWilliams, 2003, 2005]

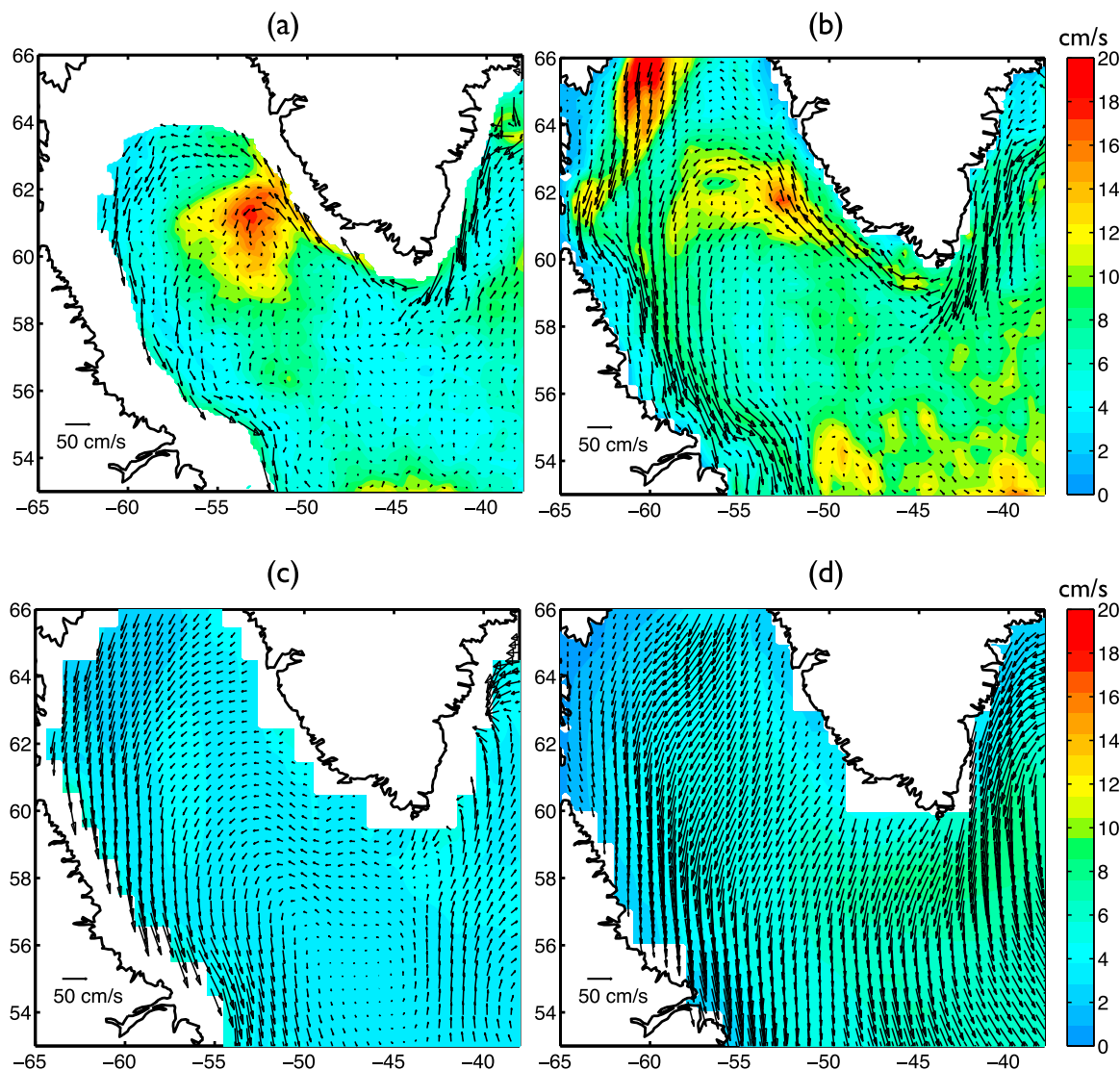


Figure 1. December to February mean distributions of surface eddy kinetic energy cast as a speed $V_{EKE} = \sqrt{2EKE}$ (in color) and mean surface velocity (arrows) over the model domain from (a) AVISO satellite altimeter data, (b) SODA 2.1.6, (c) ECCO-JPL, and (d) ECMWF ORA-S3 reanalyses.

to simulate the ocean circulation in the Labrador Sea. ROMS is a free surface, terrain-following, hydrostatic, primitive equation ocean model that has been widely used in regional and coastal circulation studies [Di Lorenzo *et al.*, 2005; Warner *et al.*, 2005; Wilkin, 2006; Haidvogel *et al.*, 2008; Luo *et al.*, 2011]. The model domain is bounded at approximately 51°N to 66°N and 35°W to 65°W (Figures 1 and 2); the horizontal resolution is 7.5 km, and there are 30 terrain-following layers in the vertical with enhanced resolution near the surface. The advection schemes implemented are third order upwind in the horizontal and fourth order centered in the vertical. Laplacian horizontal diffusion is used for momentum, temperature and salinity. In addition, a nonlocal closure scheme based on the K-Profile Parameterization (KPP) formulation [Large *et al.*, 1994] is employed at the surface boundary layer and the Large/McWilliams/Doney (LMD) scheme [Large *et al.*, 1994] parameterizes vertical mixing due to shear instability in the ocean interior.

[11] The model bathymetry is created from ETOPO2 2 min Gridded Global Relief Data Collection topography [Sandwell and Smith, 1997]. To prevent potential errors of the pressure gradient induced by s coordinate horizontal layers [Haney, 1991; Beckmann and Haidvogel, 1993; Mellor *et al.*, 1994, 1998], the bathymetry is smoothed to a maximum slope parameter r_{max} of 0.35, which is defined as a ratio of the maximum difference between adjacent grid cell depths and the mean depth at that point ($r_{max} = \Delta h/h_{mean}$). A smooth logarithmic interpolation method [Penven *et al.*, 2008] is applied everywhere without any visible suppression of modeled eddy activity except for a limited region around Cape Desolation, where we therefore retain the original data of Sandwell and Smith [1997]. Previous studies have shown that the topographic details near Cape Desolation control the boundary current meandering and subsequent shedding of Irminger Rings [Eden and Böning, 2002; Katsman *et al.*, 2004; Bracco *et al.*, 2008]. LBD11 confirmed that the

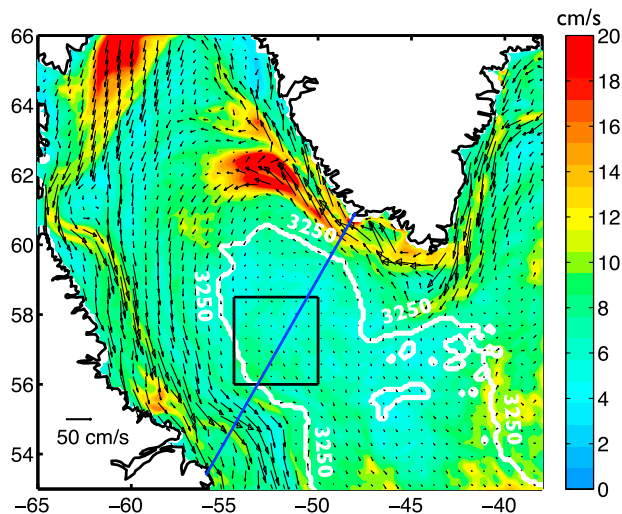


Figure 2. Model domain and boreal winter (December to February) mean distribution of surface eddy kinetic energy cast as a speed $V_{EKE} = \sqrt{2EKE}$ (in color) and mean surface velocity (arrows). The white line follows the 3250 m isobath, the blue line depicts the AR7W WOCE/CLIVAR hydrographic section, and the black box (convective box in the paper) indicates the region in which we concentrate most of the analysis of the modeled potential temperature variability.

simulated circulation is extremely sensitive to the local bathymetry in the West Greenland region and any topography smoothing along the coast can cause a significant EKE reduction in the proximity of Cape Desolation and the appearance of a secondary peak of EKE further north. By retaining all the details in ETOPO2 only along West Greenland, the model is able to better simulate the observed eddy formation and detachment toward the interior without introducing significant pressure gradient errors (see LBD11 for a comprehensive discussion of this point).

2.2. Forcing

2.2.1. Surface Forcing

[12] The model is forced with surface wind stresses and heat fluxes from the National Center for Environmental Prediction/National Center for Atmospheric Research (NCEP/NCAR) reanalysis from January 1976 to December 2009 [Kalnay et al., 1996]. To avoid long-term drifts in the SSTs associated with errors in the NCEP surface fluxes [Josey, 2001; Renfrew et al., 2002], the NCEP/NCAR surface heat fluxes are corrected using National Oceanographic and Atmospheric Administration (NOAA) extended SST [Smith and Reynolds, 2004] at a resolution of $2^\circ \times 2^\circ$ with a time scale of 1 month. Formally, the heat fluxes forcing ROMS at the surface, Q_{Mod} , are calculated according to $Q_{Mod} = Q_{Ncep} + dQ_{Mod}/dSST_{Mod} \times [SST_{Mod} - SST_{NOAA}]$, where $dQ_{Mod}/dSST_{Mod}$ quantifies the constrained net heat flux sensitivity to SST in the model.

2.2.2. Ocean Boundary Forcing

[13] Boundaries are open in the east, south and north sides of the domain and closed in the west. A modified radiation condition [Marchesiello et al., 2001, 2003] coupled with nudging to the boundary variables is prescribed along the open boundaries.

[14] There are great uncertainties in ocean reanalyses at high latitudes. Boundary conditions are particularly important in regional simulations of the Labrador Sea given the sensitivity of the basin to the incoming currents [Myers et al., 2007; Rattan et al., 2010]. In this work we have chosen SODA [Carton et al., 2005; Carton and Giese, 2008] after assessing the reliability of several reanalyses available to us. Figure 1 shows the winter mean surface currents superimposed on the EKE map over the model domain derived from Archiving, Validation, and Interpretation of Satellite Oceanographic (AVISO) altimetry data, and from Estimating the Circulation and Climate of the Ocean–Jet Propulsion Laboratory (ECCO-JPL) [Wunsch et al., 2009], Ocean Re-Analysis System 3 (ORA-S3) [Balmaseda et al., 2008] and SODA (version 2.1.6) reanalyses, over the common period 1993–2007. Comparing surface EKE patterns and current behaviors, particularly at the boundary, SODA shows better agreement, in all seasons and at interannual scales (not shown), with the satellite observations. ECCO-JPL and ORA-S3 do not resolve the localization of the boundary current system at the northeast corner of the domain, and ECCO-JPL underestimates its strength. Likely as result of a poor representation of the boundary current system, the EKE peak along the West Greenland coast in correspondence to the formation of Irminger Rings is absent in both reanalyses. We also analyzed how the data sets represent the temperature of the incoming Irminger Current at the domain boundary. The annual cycle is similar between them, with ECCO-JPL being 0.8°C warmer, and ORA-S3 being 0.7°C colder than SODA throughout the year. SODA and ORA-S3 share a similar trend in temperature anomalies, with warmer waters characterizing the 1998–2005 period compared to the previous years, while ECCO-JPL does not display any trend. All correlations of pairs of monthly time series of temperature anomalies are statistically non significant, including for two versions of SODA (SODA 2.0.2–4 and SODA 2.1.6), but SODA and ORA-S3 display similar variance, while the variability is reduced in ECCO-JPL. Ultimately, we have chosen SODA over ORA-S3 due to the limited resolution of ORA-S3 (only $1^\circ \times 1^\circ$ in the horizontal) and its inability to properly simulate the lateral extent of the boundary currents. As noticed by Rattan et al. [2010], a good representation of the advective pathways around Greenland is critical for a proper representation of the density gradients in the whole basin. The reader is referred to section 4.2 (Figure 3a) for an assessment of the performance of the three reanalyses in reproducing the interannual variability of potential temperature in the Labrador Sea.

[15] As noticed, differences between various versions of SODA are not negligible at the model domain boundary (see Figure 9 in section 5.1), and to account for uncertainty in this work, we use both SODA 2.0.2–4 and SODA 2.1.6. Those data sets are generated using different versions of the Parallel Ocean Program (POP) model (2.0 and 2.1) and assimilate all observations collected in the World Ocean Database (WOD) [Boyer et al., 2006] releases from 2005 and 2009, respectively.

[16] A first ensemble, MF_{CL} (for interannually monthly varying forcing, climatological boundary conditions), is conducted by nudging the open boundaries to monthly mean values obtained averaging the SODA monthly output from 1980 to 2006 or 2008 (see below). In this way the model boundaries retain the climatological seasonal cycle, but the interannual variability at the ocean boundaries is removed.

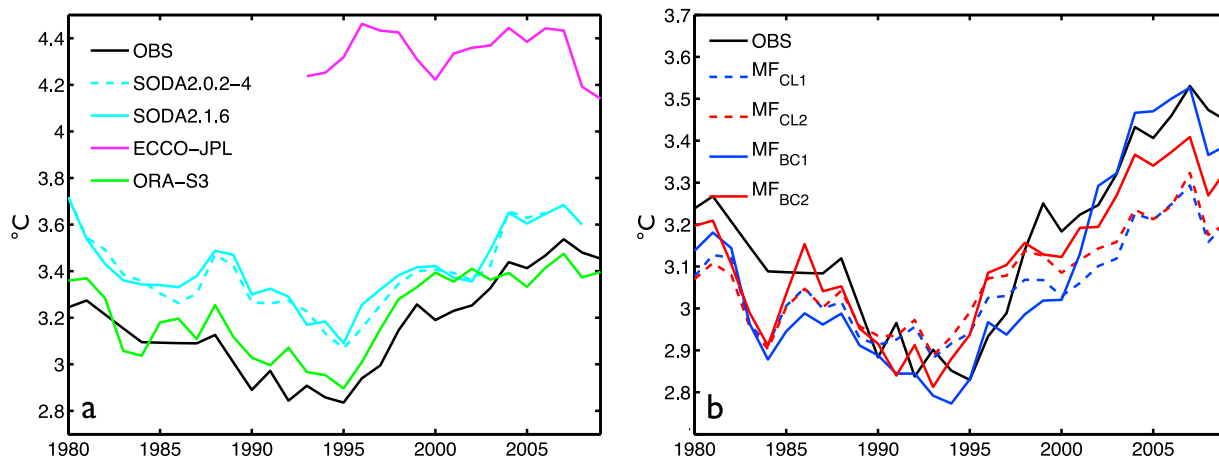


Figure 3. Annual mean of potential temperature in the region comprised by the 3250 m isobaths following *Yashayaev* [2007]: (a) reanalysis and observation and (b) models and observation. Potential temperature values are averaged over waters comprised between 150 m and 2000 m depth. Observed values are in black, ECCO-JPL in magenta, SODA 2.0.2–4 in dashed cyan, SODA 2.1.6 in cyan, ECMWF ORA-S3 in green; MF_{CL1} integration in dashed blue, MF_{CL2} in dashed red, MF_{BC1} in blue, and MF_{BC2} in red.

MF_{CL} includes two members: one uses SODA 2.0.2–4 (MF_{CL1}), the other SODA 2.1.6 (MF_{CL2}). They are both initialized at January 1976 and run through 2009. In the analysis, the first 4 years are discarded and only the period of 1980–2009 is considered.

[17] A second ensemble, MF_{BC} (for interannually monthly varying forcing and boundary conditions), is nudged to monthly varying SODA fields, retaining the interannual variability at the boundaries. Again, one member (MF_{BC1}) implements SODA 2.0.2–4 and the other (MF_{BC2}) SODA 2.1.6. SODA 2.0.2–4 ends in 2007 and the reanalysis is not reliable over the last year (http://www.atmos.umd.edu/~carton/index2_files/soda.htm). In MF_{BC1} we extend the model run to 2009 by repeating the 2006 boundary conditions for the following 3 years. For MF_{BC2} , SODA 2.1.6 ends at 2008, and we use the boundary conditions of 2008 also for 2009. The boundary that we analyze in the remainder of the discussion is the northeastern one, and particularly the northeastern corner, where the reanalysis provides temperature, salinity and velocities for the incoming Irminger Current. We verified that the velocity field does not display any significant trend in the seasonal cycle, and has limited year-to-year variability. The temperature and salinity field of the incoming Irminger Current, on the other hand, show warming and slight increase in salinity, respectively, over the 1995–2004 period, a slight cooling (0.15°C) in 2005 with a 0.2°C dip in the first few months of 2006 in both SODA versions, and no significant trend thereafter for SODA 2.1.6. By repeating the 2006 conditions in MF_{BC1} we may be introducing a cold bias over the last 3 years.

[18] Initial conditions for all integrations are derived from spin-up runs, forced by climatological monthly averaged NCEP atmospheric fluxes and SODA boundary conditions, that extend for 50 years after a stationary state has been reached.

3. Model Mean Circulation

[19] The model surface EKE and velocity vectors in winter (December to February) averaged over the period 1980–2009 are shown in Figure 2. The mean surface circulation is mainly

cyclonic with swift currents around the basin in good agreement with the satellite observations. The model results have been compared in detail to TOPEX/Poseidon satellite altimeter data in LBD11 and the reader is referred to that paper for a more detailed validation of the surface circulation throughout the year, including the model surface EKE seasonal cycle along the Greenland coast and in the convective area. Here we reiterate that the EKE maximum off the west coast of Greenland does not extend as far south as observed, as apparent by comparing Figures 1a and 2. The simulations, on the other hand, capture the closed cyclonic recirculations or counter flows at 700 m depth in the Labrador Sea interior [*Lavender et al.*, 2000], but the modeled intensity is weaker than observed.

[20] Independently of the forcing fields used, and although the horizontal resolution is just below the Rossby radius of deformation in the Labrador Sea, the model is capable of capturing the eddy variability in the basin, as shown in LBD11. The model representation of number, vertical extent and intensity of the Irminger Rings is in good agreement with the observations; IRs lifespan, however, is too short, varying from 6 to 7 months in the MF_{CL} ensemble to 8 to 11 months in the MF_{BC} runs, on average. In all integrations, modeled IRs reach the interior of the basin following two paths. The first path can be described as a slow drift in the southwest direction from the location of formation, while the second is given by a faster advective pathway within the Irminger Current along the 3000 m isobaths, in agreement with the analysis of hydrographic observations by *Rykova et al.* [2009]. ROMS appears to underestimate the first path in favor of the second one, and is unable to reproduce the observed rate of IR southward migration. As a result in the model runs fewer eddies than observed move as far south as 58°N and the EKE maximum is displaced northward. In the MF_{CL} integrations where the climatological seasonal cycle is repeated at the boundaries over the length of the integrations, the interannual variability in the shedding of Irminger Rings from the west coast of Greenland is driven by the strength of the bottom boundary current that varies chaotically due to

ocean intrinsic instability processes that take place along the east Greenland coast. In the MF_{BC} , instead, such variability is modulated by the surface component of the East Greenland Current and the resulting eddies are longer living and more intense than in MF_{CL} (LBD11). In all runs the seasonal cycle of IR production is regulated by the local atmospheric forcing. In the central Labrador Sea, our simulations reproduce a substantial portion of the observed EKE variability that appears to be controlled, both in the model and in the observations, by local sensible and latent heat losses integrated over 2–3 months. In this area at least 80% of the simulated EKE is contributed by eddies that form locally, are smaller than the Irminger Rings, and have shorter lifespan (about 3 months on average). They are predominantly anticyclonic, form around $59^{\circ}N$, preferentially during the spring season, and have been identified also in XBT sections (LBD11). It should be noted that the area defined here as central Labrador Sea differs slightly from the one in LBD11, due to differences in the data sets used for comparison with the observations. We analyzed the EKE variability in the box shown in Figure 2 (indicated as convective box in the following) and the results are consistent with our previous findings. In the convective region the surface EKE is characterized by negative anomalies from 2002 onward. Finally, modeled BCEs form along the periphery of the Labrador Sea by baroclinic instability, as suggested by the idealized studies by Spall [2004] and Straneo [2006b] (see Figure 5 of LBD11).

4. Validation of Potential Temperature Representation

4.1. Observational Data and Methods

[21] To compare the model output with observations, we sample modeled and observed potential temperature fields, and compile sets of regional indices and diagrams applying approaches and data-averaging schemes similar to those used by Yashayaev [2007] and Yashayaev and Loder [2009]. As a source for observational variables we use an extensive collection of Labrador Sea hydrographic data comprising both historic and recent data sets. For the historic (1930–2005) component of this collection we merged shipboard observations collected by Bedford Institute of Oceanography (BIO) and Fisheries and Ocean Canada (DFO) with those extracted from the international archives of hydrographic data hosted and maintained by NODC, ICES, WOCE, presently CLIVAR, and other agencies and projects. The more recent data sets used in this study are exclusively based on the annual hydrographic surveys of the Labrador Sea performed by BIO. These surveys are primarily aimed to sample the AR7W WOCE/CLIVAR line that extends from the Labrador to the Greenland shelves. The annual survey of the AR7W line started in 1990. An occupation of AR7W normally takes place in late spring to early summer (May–July), but in 1996 and 2002 BIO had cruises in fall–winter (October–December) in addition to regular spring occupations. These surveys provide invaluable measurements of physical [e.g., Lazier *et al.*, 2002; Yashayaev *et al.*, 2003; Lu *et al.*, 2006; Yashayaev, 2007; Yashayaev *et al.*, 2007a, 2007b; Yashayaev and Loder, 2009], chemical [e.g., Azetsu-Scott *et al.*, 2003] and biological [e.g., Head *et al.*, 2000]

measurements throughout the entire water column of the Labrador Sea.

[22] In the observational data products used in this work we also incorporate the profiling Argo float data, providing real-time measurements of temperature and salinity of the upper 2000 m in the Labrador Sea since June 2002. Argo observations provide a continuous in time but irregularly spaced coverage of the seawater properties in both the Labrador Sea and adjacent basins [Yashayaev and Loder, 2009]. The vertical temperature profiles obtained by Argo floats used here were downloaded from the Global Data Assembly Centers. We use a combination of real time and delayed data (whenever the latter is available), but we quality control each Argo profile (both T and S), by analyzing deviations from spatially and temporally binned medians, and we remove any profile with bad data or large data gaps. The profiles are then vertically interpolated and confined to the Labrador Sea Argo domain shown in the study of winter convection of 2007–2008 [Yashayaev and Loder, 2009]. To achieve consistency with model results presented in the paper, we grouped and averaged Argo profiles over independent 14 day bins, therefore Argo values shown here may seem smoother than in the aforementioned study.

4.2. Modeled Potential Temperature Variability

[23] The goal of this work is to investigate and attribute the interannual variability of potential temperature (PT) in the central Labrador Sea, where deep convection occurs. As a preliminary step, we need to assess the model performance against available observations and reanalyses data sets in representing the potential temperature.

[24] First of all, in Figure 3a we show the annual mean PT averaged over the upper 150 to 2000 m of the water column and in the central part of the Labrador Sea (defined here by the 3250 m isobath) in SODA (both versions), ECCO-JPL and ORA-S3 reanalyses, and in the observations, while Figure 3b compares our four model runs to the observations. The black line representing observations in Figure 3 is based on all available data. It shows a trend toward lowering from 1980 to 1992, partially interrupted by stable temperatures between 1984 and 1987, when, however, there are few hydrographic profiles and mostly located outside the convective area shown by the convective box in Figure 2, and a warming from 1995 onward. SODA, independently of the version used, is characterized by a warmer than observed mean state at all times, ECCO-JPL is too warm and is unable to reproduce any trend, while ORA-S3, despite the low horizontal resolution that does not allow for resolving the ocean mesoscale or the boundary current structure, shows very good agreement with the observations. ORA-S3 has several innovative features compared to the other reanalysis, including an online bias correction algorithm and a three-dimensional optimal interpolator scheme to assimilate all observations available in the top 2000 m of the water column, and those features may contribute to the good match. Focusing on SODA, chosen for our runs over ORA-S3 for the better representation of the boundary current structure and higher horizontal resolution, we notice that temperatures in the early 1980s were as warm as in the last decade, while in the observations they were approximately $0.2^{\circ}C$ colder at the beginning of the record than in the 21st century. Additionally, SODA underestimates all deep convection events before

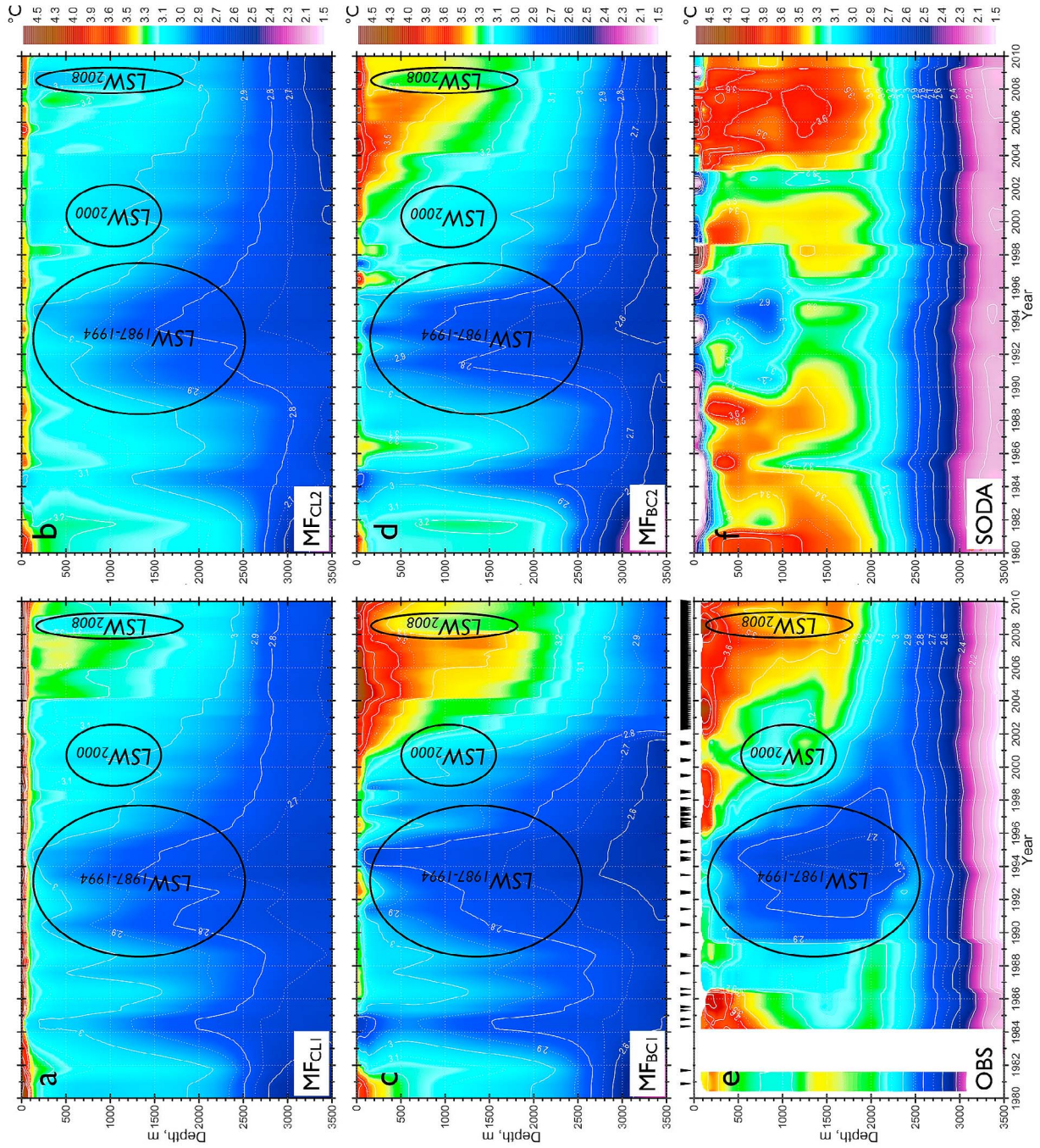


Figure 4

Table 1. Linear Trend Coefficients Describing the Decadal Variability of the Annual Mean Potential Temperature for the Observed and Modeled Time Series Shown in Figure 3

	Time Series	
	1980–1994	1995–2009
Observations	-0.40°C ($-0.027^{\circ}\text{C/yr}$)	0.65°C (0.045°C/yr)
MF _{CL1}	-0.15°C ($-0.010^{\circ}\text{C/yr}$)	0.30°C (0.020°C/yr)
MF _{CL2}	-0.20°C ($-0.013^{\circ}\text{C/yr}$)	0.25°C (0.016°C/yr)
MF _{BC1}	-0.37°C ($-0.025^{\circ}\text{C/yr}$)	0.68°C (0.047°C/yr)
MF _{BC2}	-0.30°C ($-0.021^{\circ}\text{C/yr}$)	0.50°C (0.035°C/yr)

1995 (see also Figure 4f). In Figure 3b, the MF_{CL} members display a cooling trend during the late 1980s and early 1990s and the temperature increase from 1995 to 2007. In both MF_{CL} runs, the central Labrador Sea reaches its coldest state ($\sim 2.9^{\circ}\text{C}$) in 1995. Those integrations, however, underestimate the values of PT cooling in the first half of the record (-0.15°C and -0.20°C in MF_{CL1} and MF_{CL2}, respectively, versus -0.4°C for the observations, or expressed in terms of linear trend coefficients, -0.010 and $-0.013^{\circ}\text{C/yr}$ versus $-0.027^{\circ}\text{C/yr}$) and warming in the second half (0.3°C or 0.020°C/yr for MF_{CL1}, and 0.25°C or 0.016°C/yr for MF_{CL2} versus almost 0.65°C or 0.045°C/yr for the observed time series, see Table 1). This provides evidence of the key role played by local atmospheric forcings that influence not only the surface kinetic energy [LBD11], but also interannual variability at depth: Cold winters are usually characterized by deep convection events that mix the potential temperature of the water column from the surface to up to 2000 m, while in warm winters only shallow convection events take place and the water column remained stratified below 1200 m [Avisic *et al.*, 2006]. Finally, in the MF_{BC} runs the use of SODA boundary conditions that retain the interannual variability signal further improves the comparison between modeled and observed PT. The cooling from 1980 to 1995, and the subsequent warming are now comparable to the observed values, with linear trends of -0.025 and $-0.021^{\circ}\text{C/yr}$ for the first half of the record and of 0.047 and 0.035°C/yr in the second half (Table 1), for MF_{BC1} and MF_{BC2} respectively.

[25] This provides a first hint of the crucial role played by the variability of the incoming waters in the observed warming over the last decade, as quantified later. Inconsistencies between observational and model data are evident in the 1982–1985 period, when the model produces lower PT, and are probably linked to the limited number of hydrographic profiles available for the convective region. This is supported by the agreement between our results, other simulations [Lu *et al.*, 2007; Zhu *et al.*, 2010], and ORA-S3 reanalysis.

[26] Second, in Figure 4 we compare the time evolution of the PT vertical distribution (from 0 to 3500 m depth) within 150 km from the AR7W line and confined in the region

marked by the 3250 m isobaths in the MF_{CL} (Figures 4a and 4b) and MF_{BC} members (Figures 4c and 4d), with the one compiled from all data available over the same region (Figure 4e), and SODA 2.1.6 (Figure 4f). Here, Figure 4e is obtained using profiles from the AR7W surveys and Argo data that can adequately map the top 2000 m of the water column. Times at which profiles and/or Argo data are available are shown as black triangles on top of Figure 4e. No data were available within the area described above from 1982 to 1984, given that the surveys over those years were limited to shallower waters close to the Greenland coast. In Figure 4, the model data have been first smoothed and then subsampled to match the observations. ROMS reproduces well the temporal interannual variability of the Labrador Sea Water (LSW) over the past 30 years. Deep convection was particularly intense between the late 1980s and mid-1990s; in 1993 the LSW reached its maximum depth; since 1994, the PT of the central Labrador Sea displays a steadily increase with only shallow convective events; in 2000 the warming trend was interrupted by a moderate deep convection episode (LSW₂₀₀₀). Winter convection over the following decade remained as shallow or shallower than 1200 m, reaching 1400–1600 m only during the 2007–2008 winter [Yashayaev and Loder, 2009; Våge *et al.*, 2009]. Little agreement is found between model runs and observations for the early/mid-1980s but the observational coverage is insufficient to resolve convective events for this period. Comparing MF_{BC} (Figures 4c and 4d) with MF_{CL} (Figures 4a and 4b) integrations, it is evident that the use of interannually varying boundary conditions generates a cooler LSW ($\sim 2.8^{\circ}\text{C}$ between 0 m and 800 m) in the early 1990s and also produces warmer waters in the upper 2000 m in the early 21st century, in better agreement with the observations [Yashayaev and Loder, 2009] (Figure 4e). However, all runs display PT values below 2500 m depth that are too high compared to in situ data. This discrepancy may be ascribed to the model physics (poor representation of vertical mixing at depth) and/or to insufficient model vertical resolution below 2500 m. In SODA the interannual variability is weaker than observed at depth and the seasonal cycle is too strong at the surface. Surface anomalies do not penetrate as deep as observed, convective events are underestimated in both number and intensity, and their influence on the PT at depth does not last as long as in the observations and in our regional integrations.

[27] The seasonal evolution of PT over the last decade in the central Labrador Sea, defined now as the black box in Figure 2 following Yashayaev and Loder [2009], is shown in Figure 5 for the MF_{CL} and MF_{BC} members, and in the reconstruction from the Argo profiles. Both our configurations clearly indicate that PT increased during the 2000s and successfully represent the deep convective mixing event in 2008, in agreement with the observational analysis by Yashayaev and Loder [2009] and Yashayaev and Greenan

Figure 4. Time evolution of potential temperature in the region comprised by the 3250 m isobath and within 150 km of the AR7W hydrographic line, following Yashayaev [2007] and Yashayaev and Loder [2009], in the (a) MF_{CL1}, (b) MF_{CL2}, (c) MF_{BC1}, and (d) MF_{BC2} runs over the period 1980–2009, (e) observations over the 1980–2009 interval, and (f) SODA 2.1.6 between 1980 and 2008. Periods of particularly intense or weak deep convection and the corresponding Labrador Sea Water (LSW) classes are also indicated. In Figure 4e all profiles available are shown at the top. Model outputs are subsampled to match the observational data set, and all data are smoothed over a 12 month window.

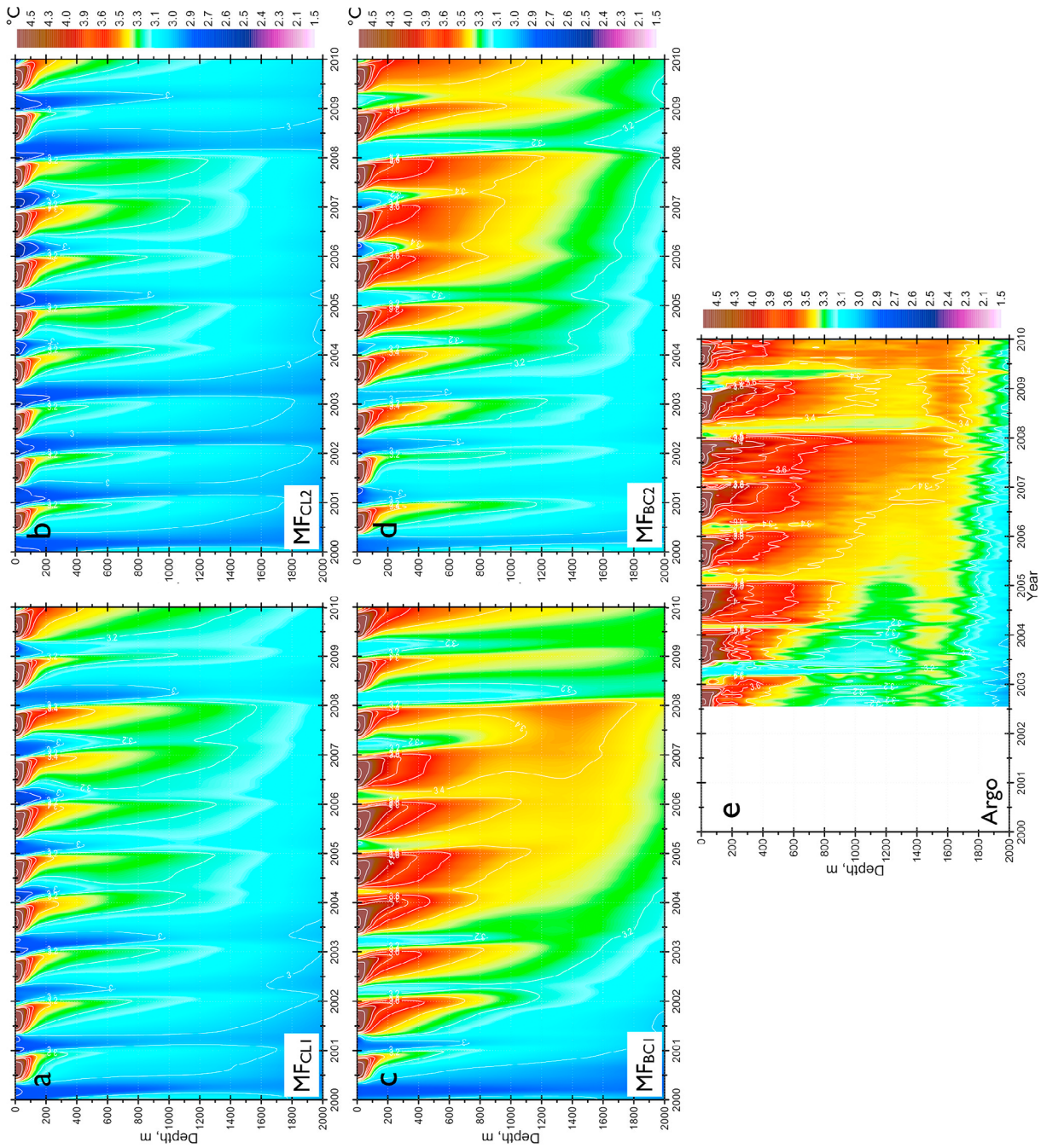


Figure 5. Seasonal-to-interannual evolution of the potential temperature in the central Labrador Sea region defined by the convective box in Figure 2 for (a) MF_{CL1}, (b) MF_{CL2}, (c) MF_{BC1}, (d) MF_{BC2} and (e) Argo profiles. The interval considered is January 2000 to December 2009 for Figures 5a–5d and July 2002 to December 2009 for Figure 5e.

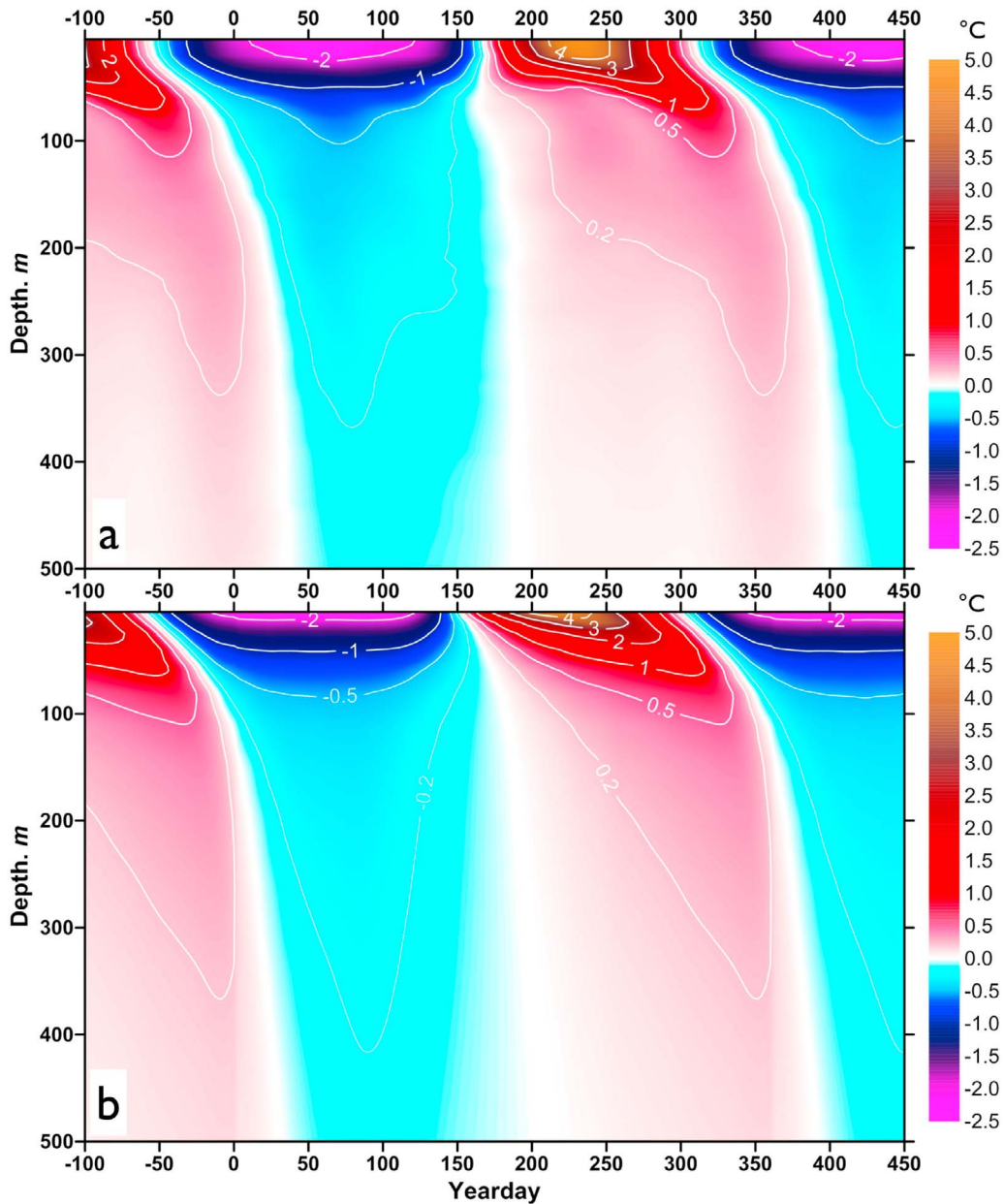


Figure 6. Seasonal cycles of potential temperature anomalies for the upper 500 m in the region defined by the black box in Figure 2 for the (a) Argo profiles and (b) MF_{BC2} integration over the 2002–2009 interval.

[2011]. As already noticed for Figure 4, both our ensembles match well the observations for depths shallower than 2000 m. The MF_{CL} ensemble reproduces only partially the observed PT trend, while the MF_{BC} captures both trend and intensity of the month-to-month variations. In the MF_{BC1} run, shown in Figure 5c, the 3.4°C isotherm reaches the depth of 1800 m in the early 2008, consistent with Argo observations, while PT at the same depth in the MF_{BC2} integration is 0.15°C warmer, indicating a sensitivity of the modeled potential temperature in the central Labrador Sea to the boundary conditions adopted. From the comparison of the two ensembles it is clear that the monthly variability of potential temperature in the central Labrador Sea is controlled by local atmospheric forcings, with the boundary conditions being the major contributor to the warming trend

over the last decade. When same climatological annual cycle is repeated every year as in the MF_{CL} ensemble, the modeled PTs underestimate the observed warming by up to 0.2°C .

[28] In Figure 6 we focus in more detail on the representation of the seasonal cycle of potential temperature anomalies with respect to the annual mean in the first 500 m of the water column as derived from Argo profiles and in the MF_{BC} ensemble. Excellent agreement between model and observations is found also when comparing the modeled heat content seasonal cycle with the analysis of PALACE floats presented by *Straneo* [2006a] over the period 1996–2000 (not shown). ROMS is therefore capable of representing correctly the seasonal cycle in periods of both moderate and weak convection.

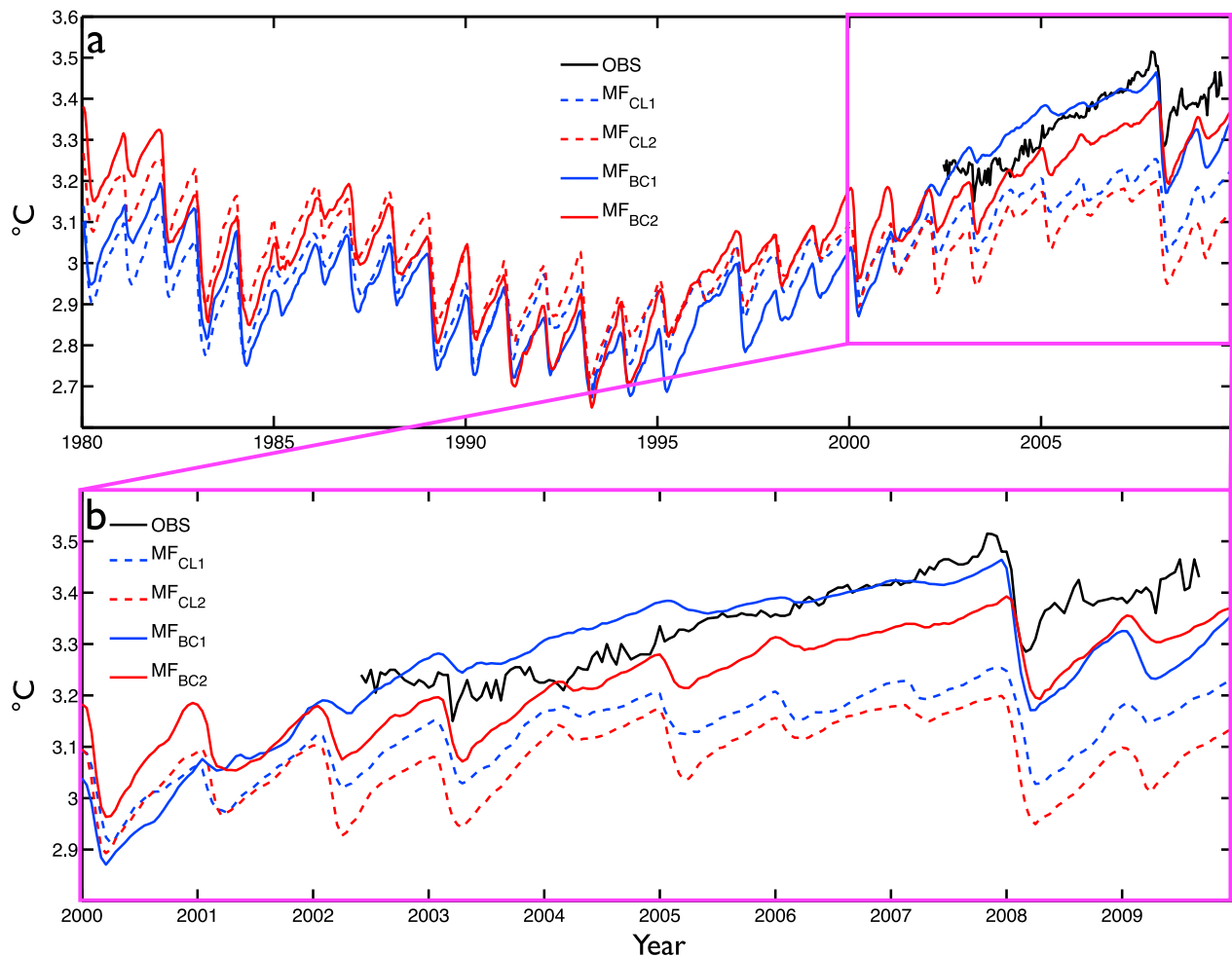


Figure 7. (a) Modeled time series of potential temperatures averaged over 1000–1500 m depth and over the black box in Figure 2 for the period 1980–2009. MF_{CL1} model output in dashed blue, MF_{CL2} in dashed red, MF_{BC1} in blue and MF_{BC2} in red. The Argo observations for 2002–2009 are also shown in black. (b) Enlarged view of the 2000 to 2009 interval, during which all integrations are characterized by a warming trend of intensity $0.018^{\circ}\text{C}/\text{yr}$ for MF_{CL1} , $0.010^{\circ}\text{C}/\text{yr}$ for MF_{CL2} , $0.039^{\circ}\text{C}/\text{yr}$ for MF_{BC1} and $0.030^{\circ}\text{C}/\text{yr}$ for MF_{BC2} , respectively. The linear warming trend for the Argo data is $0.034^{\circ}\text{C}/\text{yr}$ but limited to July 2002 onward.

[29] The comparisons between model and observations shown so far gives us confidence in the correct representation in ROMS of the timing, duration and intensity of convective events and of the restratification processes, even if the modeled Irmingier Rings have shorter lifespan than observed and not enough of them propagate as south as 58°N . A possible interpretation is that simulating correctly the number of IR is sufficient to get a good representation of the amount of water that from the boundary ends into the convective region through horizontal advection.

[30] Finally, the modeled mean PT time series calculated for depths comprised between 1000 and 1500 m over the central Labrador Sea (convective box) and the observed one from Argo profiles from June 2002 onward, are shown in Figure 7. All time series show similar tendencies, with significant temperature drops in 1983 and 1984, a continuous decrease from the 1980s to the early 1990s, and a steady increase from 1995 until 2007. In Figure 7a, no significant

differences can be seen between the modeled PT time series in the MF_{CL} and MF_{BC} ensembles during the period of 1980–2000. In spring of 2008, PT drops by over 0.2°C in both MF_{CL} and MF_{BC} runs following a deep convection event induced by the unusually cold 2007–2008 winter, which is consistent with observations. Once more, the warming trend of the last decade is not captured by the MF_{CL} runs. The MF_{CL} ensemble warms up by 0.01 – $0.018^{\circ}\text{C}/\text{yr}$ according to a linear trend calculated over the last 10 years of the time series, and underestimates the potential temperature by as much as 0.25 – 0.3°C by 2007 (Figure 7b). The MF_{BC} runs produce a better fit with the observations, with a warming trend of 0.030 – $0.039^{\circ}\text{C}/\text{yr}$ from 2000 to 2009, which is roughly consistent with Argo profile observations [Yashayaev and Loder, 2009] and moored observations of Labrador Sea outflow [Fischer et al., 2010]. Beginning in 2000 the MF_{BC} integrations display a stronger PT trend that results from the temperature increase in the water injected into the domain at the northeast boundary. All the runs

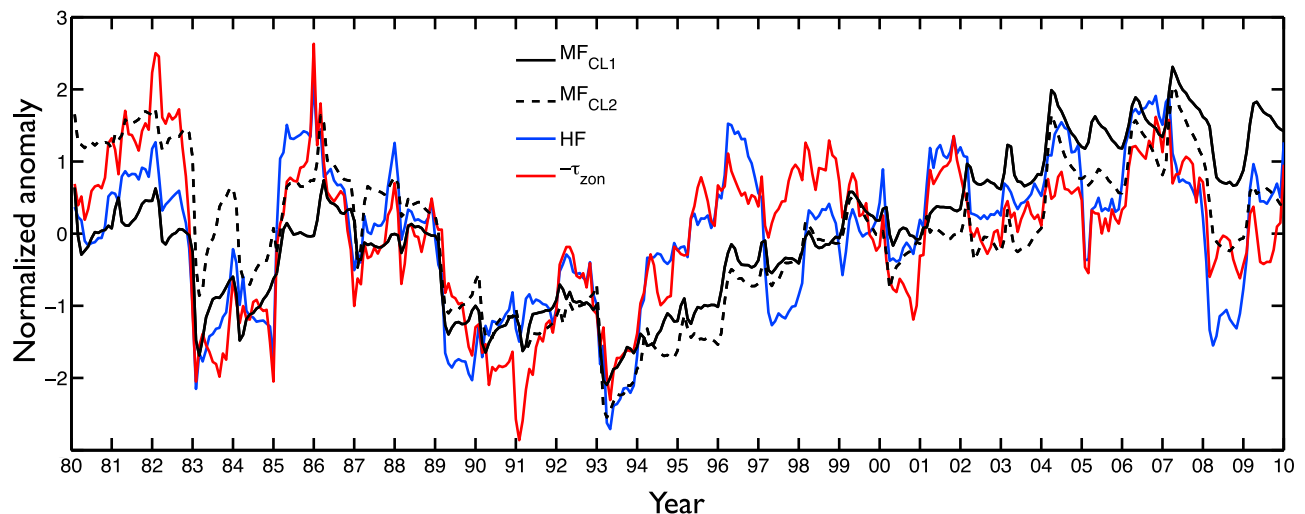


Figure 8. Time series of potential temperature anomalies for the 1980–2009 period in the MF_{CL} ensemble (in black) and local atmospheric forcing anomalies (heat fluxes in blue and zonal wind stress in red) integrated over 1 year prior from NCEP data from 1979 to 2009. All time series are normalized to have unit standard deviation.

capture the PT drop that follows the convection event during winter 2007–2008. The MF_{CL} ensemble and the MF_{BC2} integration capture well also the magnitude of the drop. MF_{BC1} , on the other hand, overestimates the temperature decrease by roughly 0.05°C . This may be due to the artificial choice of boundary conditions (in this run the boundary conditions for 2006 are repeated over the 2007–2009 period, likely introducing a cold bias). Our integrations support the conclusion that the deep convective event in winter 2007–2008 resulted from strong atmospheric cooling and local heat loss, as described by *Yashayaev and Loder* [2009] and *Våge et al.* [2009].

5. Results

5.1. Attribution of Potential Temperature Changes

[31] Summarizing the results so far, ROMS is capable of reproducing the observed variability of potential temperature in the convective region for water depths comprised between the surface and 2000 m. The atmospheric forcing plays a key role in the decadal evolution of potential temperatures at depths, determining when deep convection occurs, but variability in the incoming waters from the boundary current system is fundamental to simulate correctly the intensity of the interannual variations.

[32] As a first step to quantify the role of the heat fluxes in controlling the interannual variability of potential temperature we first look at how their time series correlates with the PT one. At the surface, LBD11 found statistically significant correlations with local wind and heat fluxes at a 2–3 month lag with the atmospheric anomalies preceding the variations in EKE, and, with lower skill, with the Arctic Oscillation (AO) index. Water temperatures at depth, however, cannot (and do not) display variance comparable to that of the atmospheric fluxes; they are affected by the atmospheric signal, integrated over time, only when the forcing is such to mix convectively to that depth, and this happens once a year or less. To insure a high statistical significance in our results,

in the following we consider the correlation between monthly PT anomalies and the local atmospheric forcing fields (e.g., heat flux and zonal wind stress) or the indices used to describe large-scale modes of atmospheric variability over the North Atlantic (e.g., the NAO and AO indices) integrating them over the preceding year. Such integration corresponds to using 1 year running mean of the atmospheric variables centered with respect to the PT anomalies 6 months earlier. For January 1980, for example, we integrate the NCEP heat fluxes for 12 months starting in January 1979, which is equivalent to take a 12 month running mean centered in July 1979.

[33] We first test the existence of a significant correlation between PT variability and the atmospheric forcing in the MF_{CL} runs. The time series of PT anomalies and of local heat and momentum flux anomalies integrated over 1 year period are shown in Figure 8. Correlations for PT anomalies and the 1 year integrated NCEP fluxes anomalies are 0.67 ± 0.01 for heat fluxes (HF), and -0.64 ± 0.03 for zonal wind stress (τ_{zon}). The statistical significance of the values above is greater or equal to 95% according to a t test. For the t test we assumed 28 degrees of freedom (i.e., the total number of simulation years, 30, minus 2). Errors are based on the intraensemble variability. Lower correlations are found using the NAO and AO indices (-0.49 ± 0.03 for the NAO curve and -0.42 ± 0.08 for the AO) (not shown), and non significant correlations are obtained when using running means calculated over periods shorter than 6 months or limited to specific seasons (for example using only winter values).

[34] For the MF_{BC} ensemble, in which interannually varying boundaries are implemented (not shown), most coefficients are slightly degraded but all still 95% statistically significant, e.g., 0.60 ± 0.01 between PT anomaly and HF, and -0.55 ± 0.05 between PT anomaly and τ_{zon} . If only the last decade is considered, however, the correlations are negligible (0.16 ± 0.02 for HF and -0.31 ± 0.06 for τ_{zon} , both integrated over 1 year). As already suggested by *Lu et al.* [2006] and confirmed by our simulations, the decadal

warming trend that started in the late 1990s in the model is linked to the warming of the incoming waters at the boundaries and cannot be explained by changes in the atmospheric forcing alone. If the time series of PT anomalies for the MF_{BC} ensemble are linearly detrended (0.021°C/yr for MF_{BC1} and 0.02°C/yr for MF_{BC2}, see Figure 7), the correlation coefficients with the 1 year integrated heat fluxes reach about 0.42 also for the last 10 years of the simulations. Given that Argo data are characterized by a comparable warming trend, we apply the same detrending procedure for the observational record (not shown). The removal of the linear trend improves the correlations between Argo PT and the local atmospheric forcing anomalies from 0.03 and -0.27 to 0.40 and -0.51 for heat fluxes and τ_{zon} , respectively, comparable to what was obtained for MF_{BC}. Due to the limited time interval covered by the observations (less than 8 years), however, we cannot assess the statistical significance of the correlations above.

[35] As already pointed out, the warming trend observed over the last decade can be properly modeled only if the boundary conditions retain the interannual variability. The relationship between PT anomalies at 1000–1500 m in the central Labrador Sea region and the incoming boundary current is analyzed in Figure 9. The cross section of the mean temperature along the eastern boundary (35°W) in SODA reanalysis is shown in Figure 9a (the mean over 30 years is similar in the two versions of SODA considered here). The cold East Greenland Current and the warm Irminger Current can be easily identified. IC water is transported into the center of the Labrador Basin by the Irminger Rings and by boundary current eddies that facilitate the exchanges of heat and fresh water between the boundary current system and the rest of the basin, as discussed in the Introduction. Interannual changes in their formation show limited variance and have been linked, in LBD11, to the shear of the incoming boundary current system imposed as boundary condition to the model domain. To begin quantifying how much the incoming Irminger Current impacts the modeled PT anomalies in the convective region, we construct time series of the potential temperature anomalies at the model boundary averaged over the IC area identified in Figures 9a and 9b in the two versions of SODA. The area encompasses the 4.7°C isotherm contour in the annual climatological average for each of the reanalyses. Those time series are then correlated in Figures 9c and 9d with the difference in PT anomalies in the convective region (black box in Figure 2) averaged between 1000 and 1500 m depth between runs retaining the interannual variability at the boundaries (MF_{BC}) and runs where boundary conditions contain the seasonal cycle but are identically repeated every year (MF_{CL}). This difference quantifies the contribution from the incoming boundary current system under the assumption that atmospheric and oceanic forcing are additive. The maximum correlation is found for the PT anomalies in the central Labrador Sea lagging the potential temperature anomalies of the Irminger Current at the model boundary by 15 months, in rough agreement with the observational estimate by Myers *et al.* [2007] of 1 year lag for IC anomalies measured at Cape Farewell (the advective time scale from the model boundary to Cape Farewell is between 75 and 80 days independently of the version of SODA used). In Figure 9c we plot the IC time series calculated at the eastern boundary of the domain for SODA 2.0.2–4 (in red),

and we compare it to the 15 month lagged time series of the central Labrador Sea PT anomalies difference between MF_{BC1} and MF_{CL1} (in blue). Figure 9d is analogous to Figure 9c but uses SODA 2.1.6 and MF_{BC2} – MF_{CL2}. Correlation coefficients are 0.68 using SODA 2.0.2–4 and 0.70 using SODA 2.1.6, and they are both 99% significant according to a *t* test. Although the IC time series differ depending on the version of the SODA reanalyses, they both show a steady warming trend from 1995 to the end of 2005.

5.2. Diagnosis of the Potential Temperature Variability

[36] We have found that the sum of the local (integrated) atmospheric forcing and the remote oceanic forcing through the Irminger Current together explain most of the variance in the interannual variability of potential temperature in the central Labrador Sea, where convection takes place, in agreement with previous analyses [Straneo, 2006a; Yashayaev, 2007]. Concentrating on the MF_{BC2} run, in this section we continue investigating the interplay between convection and restratification processes. The first is driven by the atmospheric heat fluxes, while the second is directly linked to the characteristics of the water carried from the boundary to the interior by the mesoscale circulation. Straneo [2006a] already analyzed such interplay using Ocean Weather Station Bravo data from 1964 to 1974 and P-ALACE floats from 1996 to 2000. Yashayaev and Loder [2009] attempted a heat balance calculation from the fall of 2002 to end of 2008 using Argo data. Using observations only, however, it is not possible to diagnose the interannual variability over several decades.

[37] The two main questions we wish to answer are the following: (1) Has the heat balance in the convective region in the central Labrador Sea changed in the 21st century, due to the warming trend of the Irminger waters, compared to previous years? (2) Has the amount of Irminger water carried to the convective region, and not only its temperature, changed through the 30 year period we consider?

[38] To answer question 1 we follow the approach proposed by Yashayaev and Loder [2009]. We calculate the time series of cumulative heat transfer (CHT) from the ocean, integrating progressively the total NCEP surface flux over the convective box shown in Figure 2 from the time in each year when heat loss begins (usually fall) until it ends (winter or early spring) (blue portion of top lines in Figure 10a). The integration continues through the part of the year when heat transfer is directed into the ocean (spring and summer), and it partially offsets the earlier cumulative heat loss (red portion, Figure 10a). As in the work by Yashayaev and Loder [2009], the CHT in each year is then compared with the ocean heat content (HC) in the same region, here calculated using the MF_{BC2} integration, instead of Argo profiles, over the whole 30 years and for the 10–1500 m depth range. The HC values are referenced to those at the start date of cooling and then reversed in sign to construct the relative heat content (RHC) time series shown in Figure 10a in light blue and pink for periods of net ocean cooling and warming, respectively. Not surprisingly, the modeled RHC is in very good agreement with the one calculated from the Argo profiles from the fall of 2002 to the end of 2008 [see Yashayaev and Loder, 2009, Figure 4]. More importantly, the comparison of CHT with RHC confirms both the key role played by the surface fluxes in determining the temperature variability in the Labrador

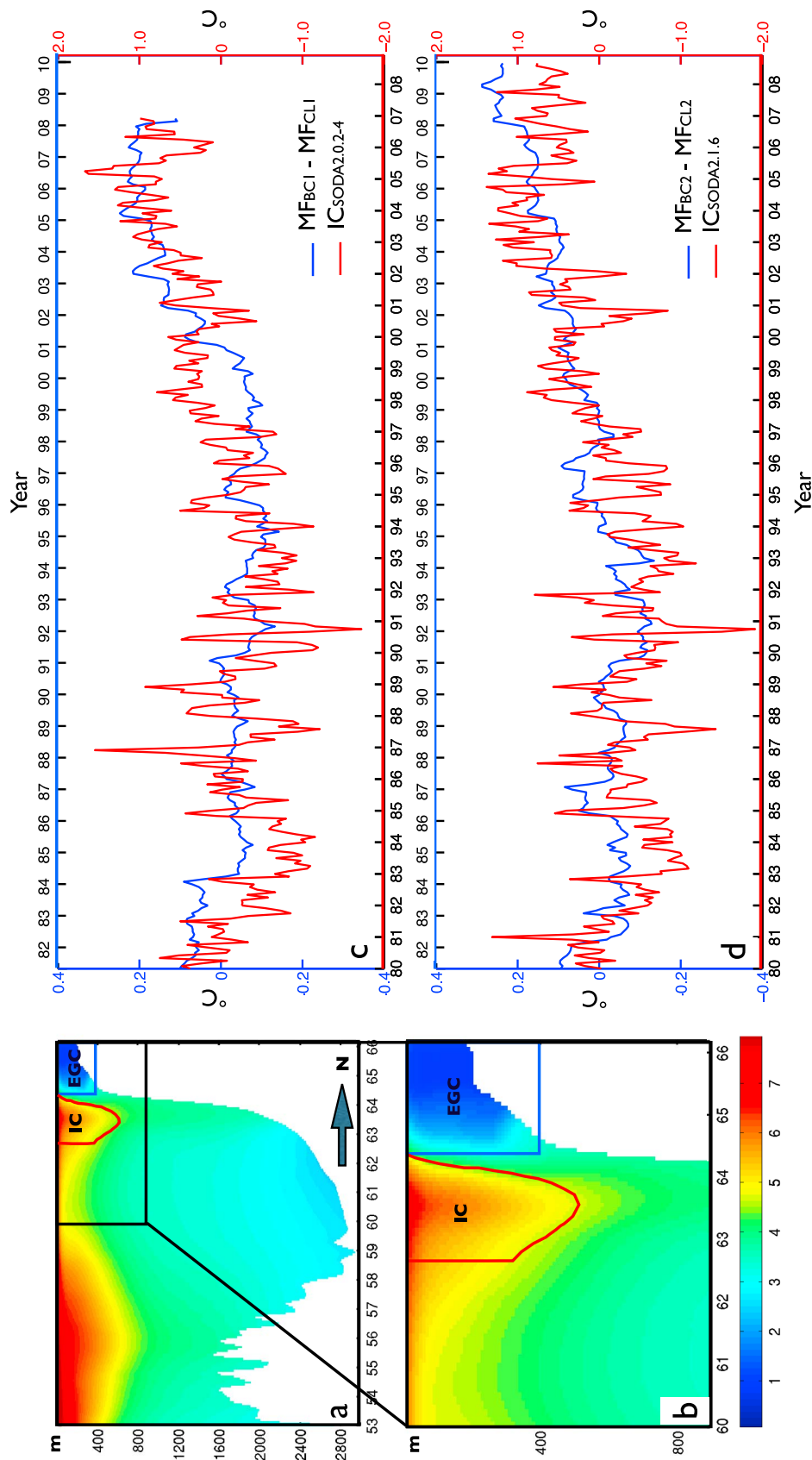


Figure 9. (a) Cross section of SODA potential temperature at the model boundary at 35°W averaged over the whole interglaciation period. The blue box highlights the East Greenland Current cold water and the red outline indicates the warmer Irmininger Current (IC). (b) Enlarged view of the upper corner of Figure 9a. (c) Time series displaying the difference between potential temperature anomalies averaged over the central Labrador Sea (convective box in Figure 2) and over 1000 to 1500 m depth in MF_{BC1} and MF_{CL1} (blue line), and the incoming IC potential temperature anomaly averaged over the red outline in Figures 9a and 9b for SODA 2.0.2-4 (red line). (d) Same as Figure 9c but for MF_{BC2} and MF_{CL2} and for the incoming IC potential temperature anomaly averaged over the red outline in Figures 9a and 9b for SODA 2.1.6. In Figures 9c and 9d the IC time series precede the central Labrador Sea one by 15 months.

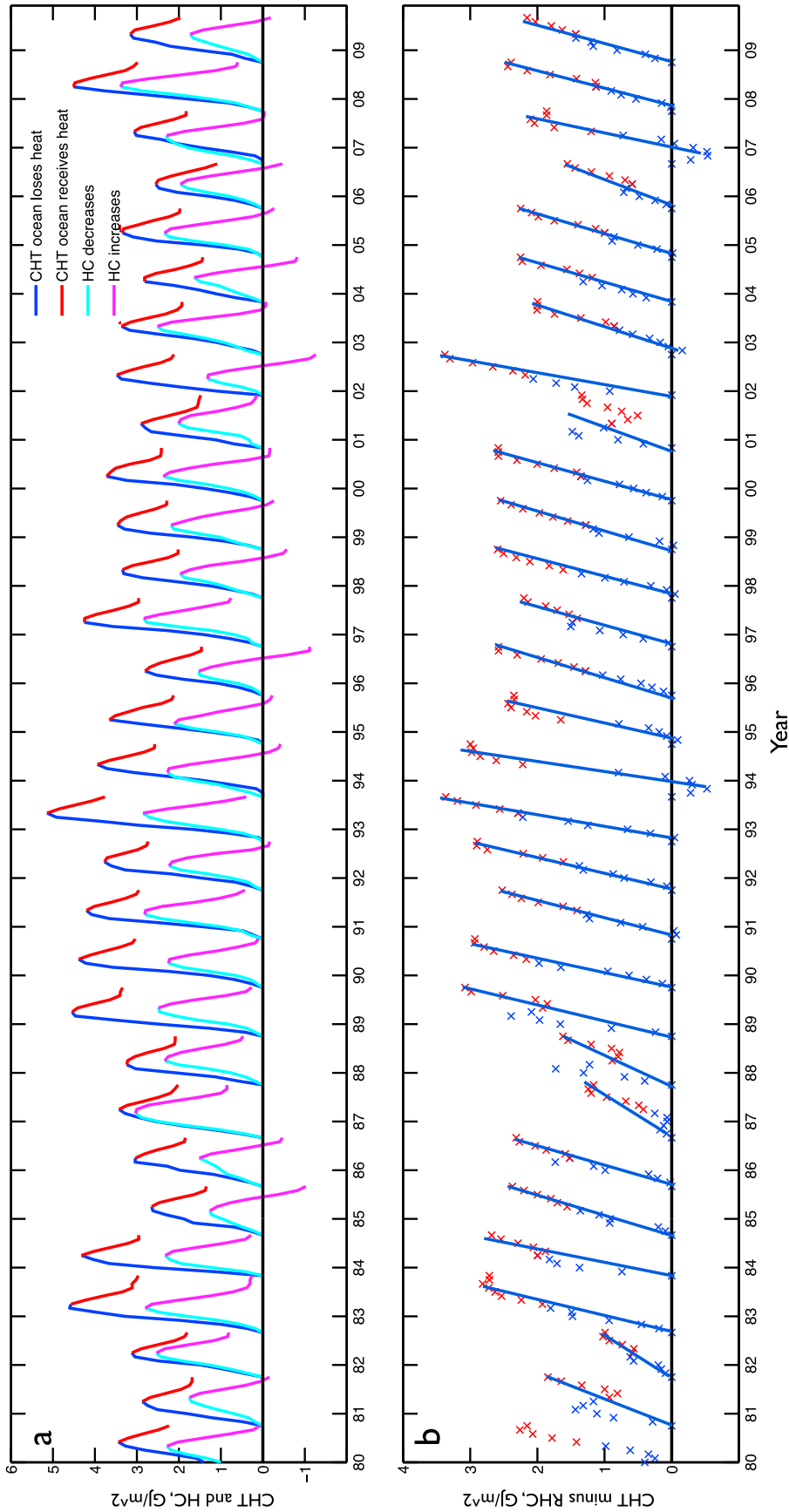


Figure 10. (a) The annual cycles of cumulative heat transfer (CHT) through the surface from the NCEP heat flux data and the ocean heat content (HC) computed using the MF_{BC2} integration over the convective box (black box in Figure 2) in the 10–1500 m depth range from 1980 to 2009. The relative heat content (RHC) is relative to the start of ocean cooling each year and reversed in sign to allow a direct comparison with CHT. (b) The differences between CHT and RHC for each cooling/warming cycle. Positive values indicate heat input to the convective box, such as lateral advection.

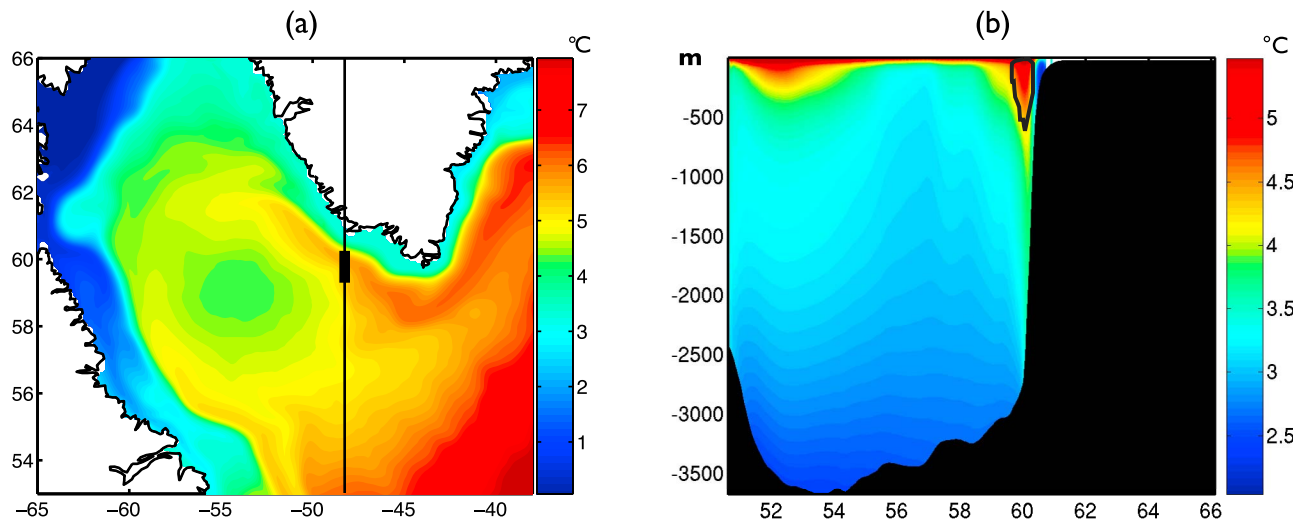


Figure 11. (a) Surface potential temperature in MF_{BC2} averaged over the whole integration period. The black box shows the location of the passive tracer release. (b) Vertical transect of the potential temperature along the black box in Figure 11a. The area delimited by the 4.7°C isotherm where the passive tracer is continuously released is highlighted.

Sea, already pointed out by *Yashayaev and Loder* [2009], and the contribution from horizontal advective-diffusive processes to the heat budget in this region, that could not be assessed in the observations due to uncertainties in the NCEP heat fluxes (being ROMS forced by NCEP fluxes, possible inconsistencies between “true” and NCEP heat fluxes are irrelevant here). The years of 1983 and 1984, 1989 to 1994, 1997 and 2008 are all characterized by large cumulative heat loss from the ocean, with CHF in 1993 being the largest with a magnitude of approximately 5 GJ/m^2 , twice as much as in 2006, when the CHF reached its minimum. Interannual variability is also found for RHC, with considerable oceanic heat gain in 1985, 1996, 2002 and 2004.

[39] The imbalance between CHF and RHC is on average 2.4 GJ/m^2 over the 30 years considered. This value is about twice as large as the previous estimate by *Straneo* [2006a]. Variations around the mean are not negligible, with values reaching 3 GJ/m^2 in 1989–1990, 1992–1994 and 2002, and values below 2 GJ/m^2 in 1981–1982, 1986–1987, 2001 and 2006 (Figure 10b). Such imbalance has to be compensated by a supply of heat from horizontal advection, and the primary source of this heat appears to be the advection of warm and salty Irminger water [*Straneo*, 2006a; *Yashayaev*, 2007; *Yashayaev and Loder*, 2009].

[40] We have shown so far that over the last decade the warming trend of the IC at the model boundary is about 1°C (Figure 9d), the warming in the convective box in Figure 2 between 1000 and 1500 m is approximately 0.3°C , about 50% of this warming cannot be explained by atmospheric forcing alone (Figure 7b), and the contribution of horizontal advection to the heat balance of the water column in the convective region is roughly constant, notwithstanding the higher than average value in 2002 (Figure 10b). All together this suggests a reduction in the overall amount of IC water stored in the convective area during the last decade compared to the previous 20 years, following the decrease in convective activity. In the model this reduction of IC water is independent of the number of Irminger Rings formed along west

Greenland; such number, indeed, does not display any significant trend in the model or in the observational record.

[41] This open issue relates to question 2 posed in this section, regarding possible changes in the amount of Irminger water carried to the convective region. To answer it, we perform a passive tracer experiment in the MF_{BC2} run. For the length of the simulation, we release continuously a passive tracer (TR_{IC} in the following) in correspondence of the Irminger Current just south of Cape Desolation, close to the west Greenland coast. The tracer injection area is kept constant and is identified by the 4.7°C isotherm in the 30 year mean average (Figure 11). This patch tracks the horizontal transport and mixing of IC water in the basin. The area where we release the tracer does not change with time in our experiment, but there is little variability in the location of the IC core. However, we may be underestimating slightly the IC contribution by defining its extension as above. TR_{IC} is first spun-up to a statistically steady distribution over the ROMS domain with an integration in which we repeat the January to December 1979 boundary and atmospheric forcing conditions for 9 years. The release is then continued for the 1980–2009 period.

[42] To quantify the IC contribution to the heat budget in the convective region of the Labrador Sea through horizontal transport, in Figure 12 we present the TR_{IC} concentration in the convective region (black box in Figure 2) for various depth ranges. In Figure 12 a concentration of, for example, 0.1 indicates that in the specified depth range 10% of water volume originated from the IC. In Figure 12 we notice that following the decrease in convective activity over the last decade, the overall amount of IC water in the convective area decreases significantly, in qualitative agreement with the conclusions of *Straneo* [2006a]. In Figure 12a, we consider the whole water column and we find concentrations varying between 8.5 and 10% from 1980 to 2002, but decreasing to values below 5% during the remaining 7 years. In the 0–1500 m range (Figure 12b), the IC concentration in the first half of the record is around 10.5%, it grows to 12.5% during

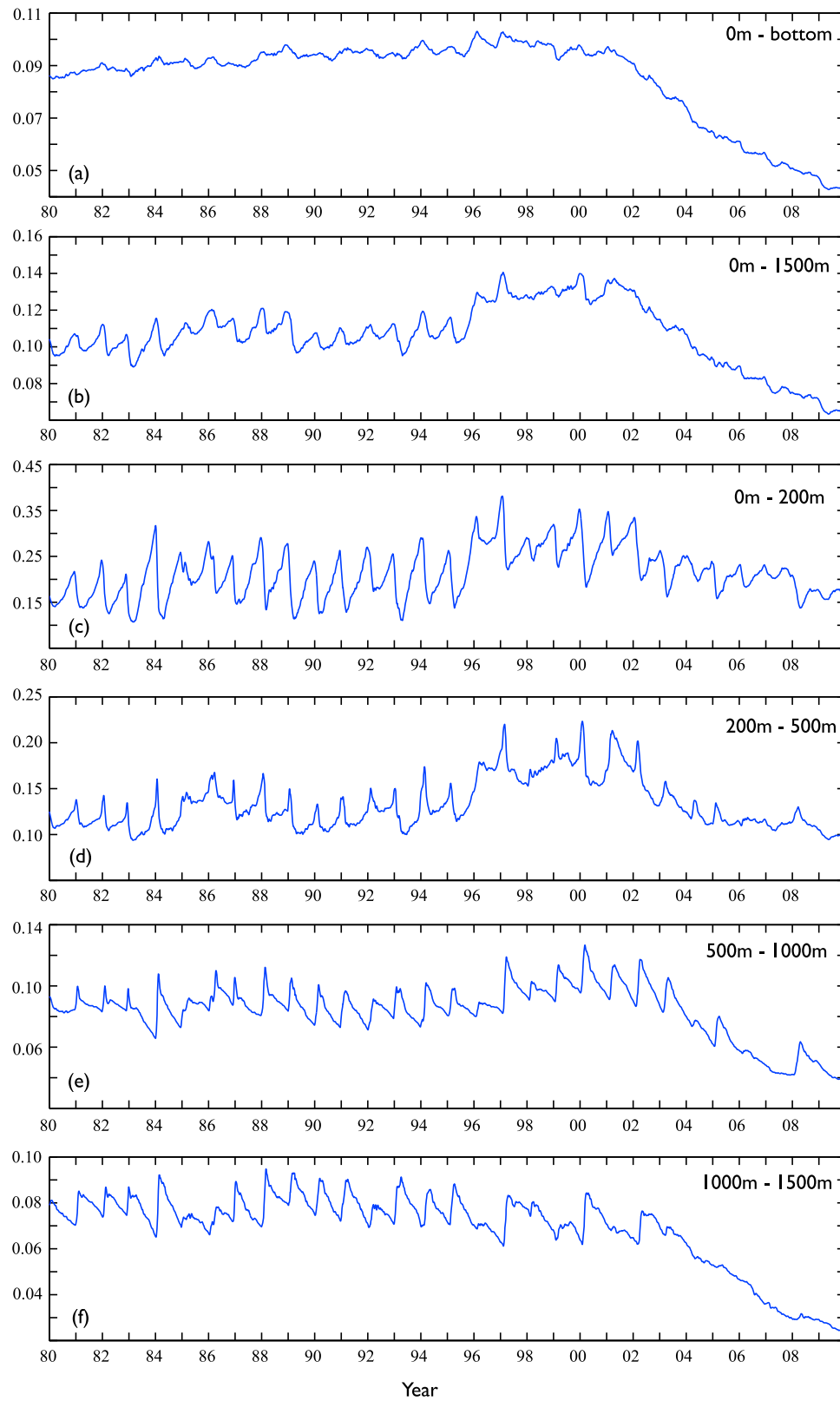


Figure 12. The mean concentration of TR_{IC} in the convective region (black box in Figure 2) for various depth ranges: (a) from 0 m to bottom, (b) from 0 m to 1500 m, (c) from 0 m to 200 m, (d) from 200 m to 500 m, (e) from 500 m to 1000 m, and (f) from 1000 m to 1500 m.

the next 6 years and drops to less than 7% by the end of 2009. In the 1000–1500 m depth range (Figure 12f) yearly averaged concentrations are around 8% until 1996, they decrease by just over half point in the following 6 years, and then plunge to values below 3% by the end of the record, with a small recovery in 2008. Despite the decrease, however, the amount of IC water found in this depth range over the last decade is sufficient to explain 42% of the warming shown in Figure 7. In correspondence to the decrease from 1996 to 2002, we find an increase in the IC concentrations in the 500–1000 m range (Figure 12e). Close to the surface (Figures 12c and 12d), on the other hand, the interannual variability in the concentration of IC water is small through the whole period, with slightly higher concentrations than average during 1996–2006. Changes are more evident in the seasonal cycle of IC concentration, which is very large in the first few hundred meters of the water column in the first 22 years of the record, and is reduced in the absence of deep convection. The seasonal cycle at depth is characterized by a sharp increase in concentration in conjunction with convective events, and a decrease during the following months, while the opposite happens in the layers close to the surface, where mesoscale advection brings IC water through the year that is then removed from the upper layers when convection occurs.

[43] This analysis suggests that the amount of IC water transported by mesoscale dynamics into the convective region in the first 500 m of the water column remained more or less constant throughout the period considered, notwithstanding a moderate increase between 1996 and 2002. In the absence of deep convective events, TR_{IC} water is confined to the upper 500 m and is flushed in and out of the convective region within a few months by the mean circulation. When deep convection occurs, on the other hand, the TR_{IC} is transported to depth by convective mixing; Once at depth, it can take up to a couple of years before it is all advected outside the area, allowing for larger overall concentrations. This is further confirmed by looking at the monthly transects of tracer concentration shown in Figure 13 for 1993 (intense deep convection year) and 2004 (no deep convection). In Figure 13 the tracer concentration is averaged over the latitudinal range of the convective box in Figure 2. Comparing Figures 13a and 13b, it is also clear that the water column is less stratified following a deep convection episode (and for a sufficiently long time to precondition the following winter convective event) than after several years of shallow or no convection.

6. Discussion and Conclusion

[44] In this paper, we investigated the interannual variability of potential temperature in the convective region in the central Labrador Sea over the last 30 years (1980–2009) with an eddy resolving regional ocean model, ROMS. The modeled ocean circulation is driven by atmospheric surface forcing fields (heat and momentum fluxes) from the NCEP/NCAR reanalysis, and the oceanic boundary conditions are derived from SODA. We have shown that our model reproduces reasonably well the variations of potential temperature in the central Labrador Sea, as recorded by hydrographic observations and Argo profiling floats. This is achieved despite an imperfect representation of the interannual variability of Irminger Rings formation (LBD11). ROMS indeed

simulates correctly the average number, seasonality and vertical and horizontal extension of those eddies, but underestimates their life span and meridional drift.

[45] With a suite of integrations we separated the influence of the incoming boundary current waters from the forcing exerted by the atmosphere. The MF_{CL} simulations are characterized by oceanic boundary conditions in which the climatological seasonal cycle is identically repeated over the length of the integrations, and the interannual variations of potential temperature of the incoming boundary current are neglected. Despite their limitations, those runs successfully reproduce a significant percentage of the observed variability and improve the representation of potential temperature variability and mean state in the central Labrador Sea compared to SODA. Such improvement is likely due to a better representation of convective vertical mixing and lateral transport in the regional model. Additionally, they show that the local atmospheric fluxes are the main driver of the interannual variability of deep convection, in agreement with what hypothesized by *Yashayaev and Loder* [2009] and *Våge et al.* [2009]. LBD11 demonstrated that in the central Labrador Sea a large portion of the interannual variability of the surface EKE is due to small eddies formed in the interior of the basin, and is forced by local atmospheric forcing; here we show that such forcing plays a major role also in modulating the changes of the depth-integrated potential temperature.

[46] The MF_{CL} configuration, however, underestimates by about $0.02\text{--}0.025^\circ\text{C}/\text{yr}$ the warming trend observed at depth during the last decade. A substantial portion of this warming is indeed contributed by the advection of boundary current waters through lateral mixing by mesoscale eddies [*Khatiwalala and Visbeck*, 2000; *Avsic et al.*, 2006] and then by vertical mixing from the upper 200–300 m to great depths when convection takes place. By implementing monthly varying the SODA boundary conditions, the MF_{BC} runs reproduce the observed (decadal) warming trend with the correct amplitude.

[47] *Schott et al.* [2009] have reported that the SODA reanalysis can successfully produce the meridional overturning circulation strength and annual changes in the CFC-11 tracer distribution. Here, we find that two of the most recent versions of SODA reanalysis overestimate the observed potential temperature in the central Labrador Sea by $0.15\text{--}0.2^\circ\text{C}$ and are unable to capture the details of the interannual variations and deep convection events before 1995, while providing good enough boundary conditions to properly simulate the warming by the Irminger waters.

[48] The analysis of the heat flux balance for the convective region reveals that the horizontal input of heat to the Labrador Sea interior over the last decade has not changed proportionally to the increase in temperature of the Irminger Current. The absence of deep convection for most of the recent years has reduced the content of IC water in the Labrador Sea interior by confining it to the surface 200–300 m. With a passive tracer experiment we found that the amount of IC water in the convective region decreased by approximately 50% between 2000 and 2009 when considering the whole water column, while remaining more or less constant in the layers close to the surface.

[49] In summary, our integrations indicate that in the central Labrador Sea the local atmospheric forcing holds primary responsibility for modulating the Labrador Sea Water

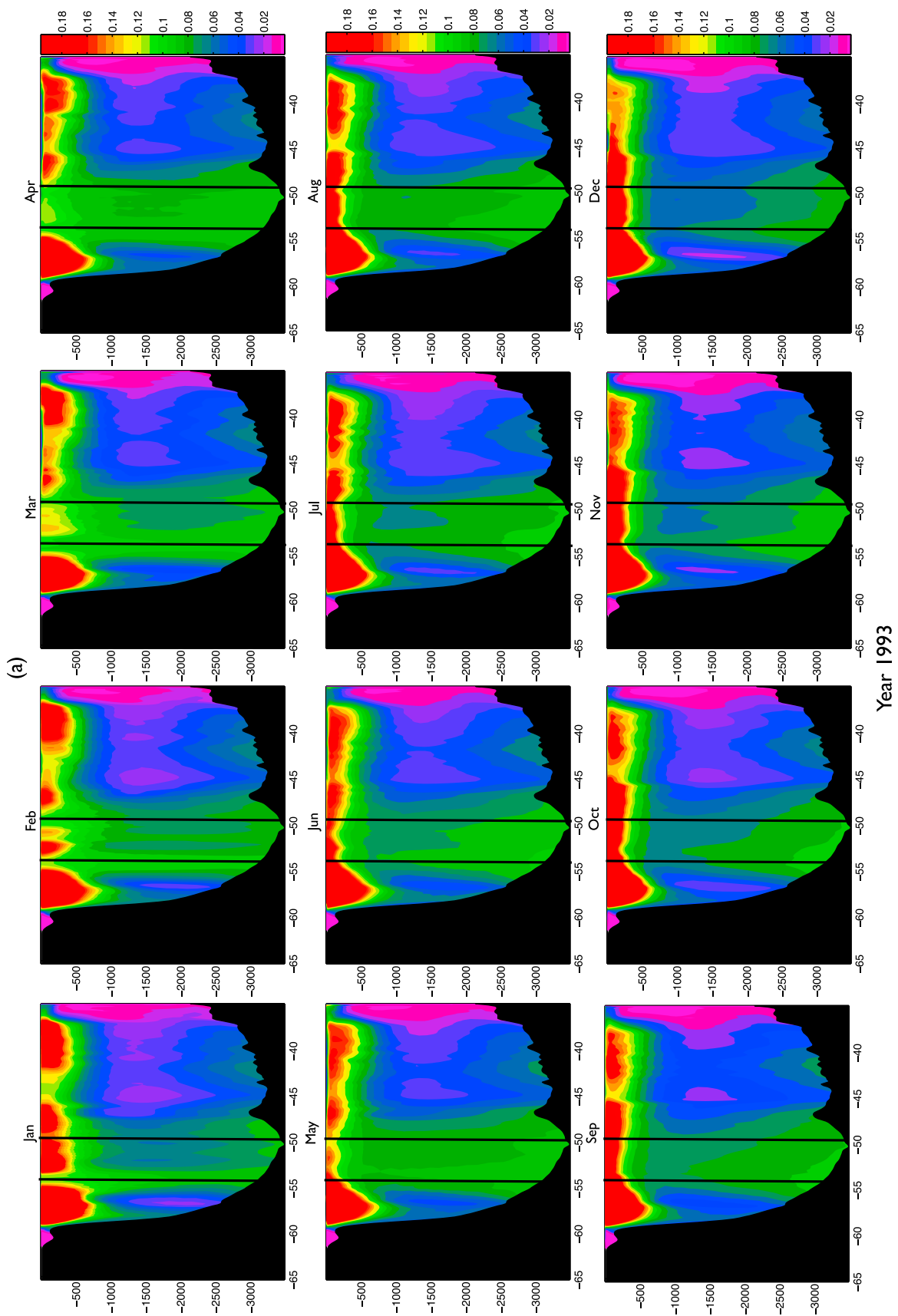
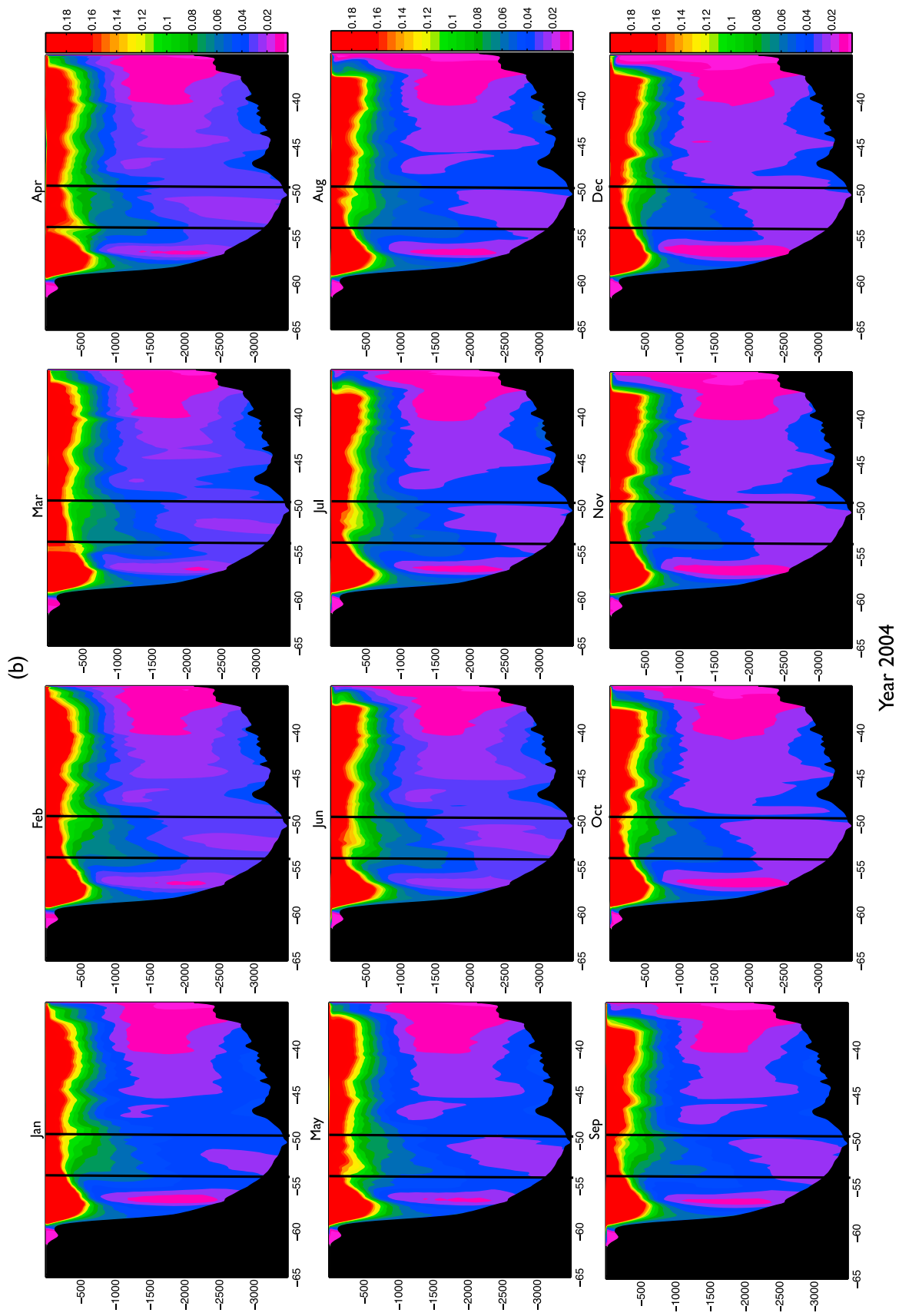


Figure 13. Monthly vertical transects showing the evolution of the TR_{1C} tracer concentration in (a) 1993 and (b) 2004. The tracer concentration is averaged over the latitudinal range of the convective box in Figure 2.



formation. The restratification of the Labrador Basin by IC water is essential to the overall water mass distributions in the center of the basin, but does not affect significantly its year-to-year variability before the last decade. In the 21st century, however, the boundary waters transported to the center of the basin by horizontal mesoscale advection and Irminger Rings contribute to about 50% of the raise in potential temperature observed at depth. This temperature increase results from the fast and substantial warming experienced by the IC current. The warming is large enough to overcome the decrease in the overall amount of IC water transported convectively below 500 m in the Labrador Sea interior. In the last decade, the IC water found in the convective region below 500 m is less than half than in the previous 20 years.

[50] **Acknowledgments.** We wish to thank three anonymous reviewers for their insightful and careful comments that helped improving this manuscript. This work was partially supported by the NSF grant OCE-0751775. Monitoring of the AR7W line in the Labrador Sea started in 1990 as a contribution of Fisheries and Oceans Canada (DFO) to WOCE and this is now a core component of DFO's Atlantic Zone Off-Shelf Monitoring Program (AZOMP) (<http://www.bio.gc.ca/science/monitoring-monitorage/azomp-pmzao/azomp-pmzao-eng.php>).

References

- Avsic, T., J. Karstensen, U. Send, and J. Fischer (2006), Interannual variability of newly formed Labrador Sea Water from 1994 to 2005, *Geophys. Res. Lett.*, **33**, L21S02, doi:10.1029/2006GL026913.
- Azetsu-Scott, K., E. P. Jones, I. Yashayaev, and R. M. Gershey (2003), Time series study of CFC concentrations in the Labrador Sea during deep and shallow convection regimes (1991–2000), *J. Geophys. Res.*, **108**(C11), 3354, doi:10.1029/2002JC001317.
- Balmaseda, M. A., A. Vidard, and D. L. T. Anderson (2008), The ECMWF Ocean Analysis System: ORA-S3, *Mon. Weather Rev.*, **136**, 3018–3034, doi:10.1175/2008MWR2433.1.
- Beckmann, A., and D. Haidvogel (1993), Numerical simulation of flow around a tall isolated seamount: Part I: Problem formulation and model accuracy, *J. Phys. Oceanogr.*, **23**, 1736–1753, doi:10.1175/1520-0485(1993)023<1736:NSOFAA>2.0.CO;2.
- Bersch, M. (2002), North Atlantic Oscillation–induced changes of the upper layer circulation in the northern North Atlantic Ocean, *J. Geophys. Res.*, **107**(C10), 3156, doi:10.1029/2001JC000901.
- Böning, C. W., M. Scheinert, J. Dengg, A. Biastoch, and A. Funk (2006), Decadal variability of subpolar gyre transport and its reverberation in the North Atlantic overturning, *Geophys. Res. Lett.*, **33**, L21S01, doi:10.1029/2006GL026906.
- Boyer, T. P., J. I. Antonov, H. E. Garcia, D. R. Johnson, R. A. Locarnini, A. V. Mishonov, M. T. Pitcher, O. K. Baranova, and I. V. Smolyar (2006), *World Ocean Database 2005* [DVDs], *NOAA Atlas NESDIS*, vol. 60, edited by S. Levitus, 190 pp., U.S. Govt. Print. Off., Washington, D. C.
- Bracco, A., and J. Pedlosky (2003), Vortex generation by topography in locally unstable baroclinic flows, *J. Phys. Oceanogr.*, **33**, 207–219, doi:10.1175/1520-0485(2003)033<0207:VGBTIL>2.0.CO;2.
- Bracco, A., J. Pedlosky, and R. S. Pickart (2008), Eddy formation near the west coast of Greenland, *J. Phys. Oceanogr.*, **38**, 1992–2002, doi:10.1175/2008JPO3669.1.
- Carton, J. A., and B. S. Giese (2008), A reanalysis of ocean climate using Simple Ocean Data Assimilation (SODA), *Mon. Weather Rev.*, **136**, 2999–3017, doi:10.1175/2007MWR1978.1.
- Carton, J. A., B. S. Giese, and S. A. Grodsky (2005), Sea level rise and the warming of the oceans in the Simple Ocean Data Assimilation (SODA) ocean reanalysis, *J. Geophys. Res.*, **110**, C09006, doi:10.1029/2004JC002817.
- Chanut, J., B. Barnier, W. Large, L. Debreu, T. Penduff, J. M. Molines, and P. Mathiot (2008), Mesoscale eddies in the Labrador Sea and their contribution to convection and re-stratification, *J. Phys. Oceanogr.*, **38**, 1617–1643, doi:10.1175/2008JPO3485.1.
- Clarke, R. A., and J. C. Gascard (1983), The formation of Labrador Sea Water, part I: Large-scale process, *J. Phys. Oceanogr.*, **13**, 1764–1778, doi:10.1175/1520-0485(1983)013<1764:TFOLSW>2.0.CO;2.
- Dickson, R., J. Lazier, J. Meincke, P. Rhines, and J. Swift (1996), Long-term coordinated changes in the convective activity of the North Atlantic, *Prog. Oceanogr.*, **38**, 241–295, doi:10.1016/S0079-6611(97)00002-5.
- Dickson, R., I. Yashayaev, J. Meincke, W. Turrell, S. Dye, and J. Holfort (2002), Rapid freshening of the deep North Atlantic Ocean over the past four decades, *Nature*, **416**, 832–837, doi:10.1038/416832a.
- Dickson, R., R. Curry, and I. Yashayaev (2003), Recent changes in the North Atlantic, *Philos. Trans. R. Soc. A*, **361**, 1917–1934, doi:10.1098/rsta.2003.1237.
- Di Lorenzo, E., M. G. G. Foreman, and W. R. Crawford (2005), Modeling the generation of Haida eddies, *Deep Sea Res., Part II*, **52**, 853–873, doi:10.1016/j.dsr2.2005.02.007.
- Eden, C., and C. Böning (2002), Sources of eddy kinetic energy in the Labrador Sea, *J. Phys. Oceanogr.*, **32**, 3346–3363, doi:10.1175/1520-0485(2002)032<3346:SOEKEI>2.0.CO;2.
- Fischer, J., M. Visbeck, R. Zantopp, and N. Nunes (2010), Interannual to decadal variability of outflow from the Labrador Sea, *Geophys. Res. Lett.*, **37**, L24610, doi:10.1029/2010GL045321.
- Fratantoni, P. S., and R. S. Pickart (2007), The western North Atlantic shelf-break current system in summer, *J. Phys. Oceanogr.*, **37**, 2509–2533, doi:10.1175/JPO3123.1.
- Gascard, J. C., and R. A. Clarke (1983), The formation of Labrador Sea Water, part II: Mesoscale and Smaller-scale processes, *J. Phys. Oceanogr.*, **13**, 1779–1797, doi:10.1175/1520-0485(1983)013<1779:TFOLSW>2.0.CO;2.
- Gelderloos, R., C. A. Katsman, and S. S. Drijfhout (2011), Assessing the role of three eddy types in restratifying the Labrador Sea after deep convection, *J. Phys. Oceanogr.*, **41**, 2102–2119, doi:10.1175/JPO-D-11-054.1.
- Haidvogel, D. B., et al. (2008), Ocean forecasting in terrain-following coordinates: Formulation and skill assessment of the Regional Ocean Modeling System, *J. Comput. Phys.*, **227**(7), 3595–3624, doi:10.1016/j.jcp.2007.06.016.
- Häkkinen, S., and P. B. Rhines (2004), Decline of subpolar North Atlantic circulation during the 1990s, *Science*, **304**, 555–559, doi:10.1126/science.1094917.
- Han, G., K. Ohashi, N. Chen, P. G. Myers, N. Nunes, and J. Fischer (2010), Decline and partial rebound of the Labrador Current 1993–2004: Monitoring ocean currents from altimetric and conductivity-temperature-depth data, *J. Geophys. Res.*, **115**, C12012, doi:10.1029/2009JC006091.
- Haney, R. L. (1991), On the pressure gradient force over steep topography in sigma coordinate ocean models, *J. Phys. Oceanogr.*, **21**, 610–619, doi:10.1175/1520-0485(1991)021<0610:OTPGFO>2.0.CO;2.
- Hätún, H., C. C. Eriksen, and P. B. Rhines (2007), Buoyant eddies entering the Labrador Sea observed with gliders and altimetry, *J. Phys. Oceanogr.*, **37**, 2838–2854, doi:10.1175/2007JPO3567.1.
- Head, E. J. H., L. R. Harris, and R. W. Campbell (2000), Investigations on the ecology of *Calanus* spp. in the Labrador Sea. I. Relationship between the phytoplankton bloom and reproduction and development of *Calanus finmarchicus* in spring, *Mar. Ecol. Prog. Ser.*, **193**, 53–73, doi:10.3354/meps193053.
- Holland, D. M., R. H. Thomas, B. de Young, M. H. Ribergaard, and B. Lyberth (2008), Acceleration of Jakobshavn Isbræ triggered by warm subsurface Irminger waters, *Nat. Geosci.*, **1**, 659–664, doi:10.1038/ngeo316.
- Jones, H., and J. Marshall (1997), Restratification after deep convection, *J. Phys. Oceanogr.*, **27**, 2276–2287, doi:10.1175/1520-0485(1997)027<2276:RADC>2.0.CO;2.
- Josey, S. A. (2001), A comparison of ECMWF, NCEP-NCAR, and SOC surface heat fluxes with moored buoy measurements in the subduction region of the northeast Atlantic, *J. Clim.*, **14**(8), 1780–1789, doi:10.1175/1520-0442(2001)014<1780:ACOENN>2.0.CO;2.
- Kalnay, E., et al. (1996), The NCEP/NCAR 40-year reanalysis project, *Bull. Am. Meteorol. Soc.*, **77**, 437–471, doi:10.1175/1520-0477(1996)077<0437:TNYRP>2.0.CO;2.
- Katsman, C. A., M. A. Spall, and R. S. Pickart (2004), Boundary current eddies and their role in the restratification of the Labrador Sea, *J. Phys. Oceanogr.*, **34**, 1967–1983, doi:10.1175/1520-0485(2004)034<1967:BEATR>2.0.CO;2.
- Khatiwala, S., and M. Visbeck (2000), An estimate of the eddy-induced circulation in the Labrador Sea, *Geophys. Res. Lett.*, **27**, 2277–2280, doi:10.1029/1999GL011073.
- Large, W. G., J. C. McWilliams, and S. C. Doney (1994), Oceanic vertical mixing: A review and a model with a non-local boundary layer parameterization, *Rev. Geophys.*, **32**(4), 363–403, doi:10.1029/94RG01872.
- Lavender, K. L., R. E. Davis, and W. B. Owens (2000), Mid-depth recirculation observed in the interior Labrador and Irminger seas by direct velocity measurements, *Nature*, **407**, 66–69, doi:10.1038/35024048.

- Lavender, K. L., R. E. Davis, and W. B. Owens (2002), Observations of open-ocean deep convection in the Labrador Sea from subsurface floats, *J. Phys. Oceanogr.*, *32*, 511–526, doi:10.1175/1520-0485(2002)032<0511:OOOOC>2.0.CO;2.
- Lazier, J. (1980), Oceanographic conditions at ocean weather ship *Bravo*, 1964–1974, *Atmos. Ocean*, *18*, 227–238, doi:10.1080/07055900.1980.9649089.
- Lazier, J., R. Hendry, A. Clarke, I. Yashayaev, and P. Rhines (2002), Convection and restratification in the Labrador Sea, 1990–2000, *Deep Sea Res., Part I*, *49*, 1819–1835, doi:10.1016/S0967-0637(02)00064-X.
- Lilly, J. M., P. B. Rhines, F. Schott, K. Lavender, J. Lazier, U. Send, and E. D'Asaro (2003), Observations of the Labrador Sea eddy field, *Prog. Oceanogr.*, *59*, 75–176, doi:10.1016/j.pocean.2003.08.013.
- Lohmann, K., H. Drange, and M. Bentsen (2009), A possible mechanism for the strong weakening of the North Atlantic subpolar gyre in the mid-1990s, *Geophys. Res. Lett.*, *36*, L15602, doi:10.1029/2009GL039166.
- Lu, Y., D. G. Wright, and R. A. Clarke (2006), Modelling deep seasonal temperature changes in the Labrador Sea, *Geophys. Res. Lett.*, *33*, L23601, doi:10.1029/2006GL027692.
- Lu, Y., D. G. Wright, and I. Yashayaev (2007), Modelling hydrographic changes in the Labrador sea over the past five decades, *Prog. Oceanogr.*, *73*, 406–426, doi:10.1016/j.pocean.2007.02.007.
- Luo, H., A. Bracco, and E. Di Lorenzo (2011), The interannual variability of the surface eddy kinetic energy in the Labrador Sea, *Prog. Oceanogr.*, *91*, 295–311, doi:10.1016/j.pocean.2011.01.006.
- Marchesiello, P., J. C. McWilliams, and A. Shchepetkin (2001), Open boundary conditions for long-term integration of regional oceanic models, *Ocean Modell.*, *3*, 1–20, doi:10.1016/S1463-5003(00)00013-5.
- Marchesiello, P., J. C. McWilliams, and A. Shchepetkin (2003), Equilibrium structure and dynamics of the California current system, *J. Phys. Oceanogr.*, *33*(4), 753–783, doi:10.1175/1520-0485(2003)33<753:ESADOT>2.0.CO;2.
- Marsh, R., S. A. Josey, B. A. de Cuevas, L. J. Redbourn, and G. D. Quartly (2008), Mechanisms for recent warming of the North Atlantic: Insights gained with an eddy-permitting model, *J. Geophys. Res.*, *113*, C04031, doi:10.1029/2007JC004096.
- Marshall, J., and F. Schott (1999), Open-ocean convection: Observations, theory, and models, *Rev. Geophys.*, *37*, 1–64, doi:10.1029/98RG02739.
- Mellor, G. L., T. Ezer, and L. Y. Oey (1994), The pressure gradient conundrum of sigma coordinate ocean models, *J. Atmos. Oceanic Technol.*, *11*, 1126–1134, doi:10.1175/1520-0426(1994)011<1126:TPGCOS>2.0.CO;2.
- Mellor, G. L., L. Y. Oey, and T. Ezer (1998), Sigma coordinate pressure gradient errors and the seamont problem, *J. Atmos. Oceanic Technol.*, *15*(5), 1122–1131, doi:10.1175/1520-0426(1998)015<1122:SCPGEA>2.0.CO;2.
- Myers, P. G., N. Kulan, and M. H. Ribergaard (2007), Irminger water variability in the West Greenland Current, *Geophys. Res. Lett.*, *34*, L17601, doi:10.1029/2007GL030419.
- Penven, P., P. Marchesiello, L. Debreu, and J. Lefèvre (2008), Software tools for pre- and post-processing of oceanic regional simulations, *Environ. Model. Software*, *23*, 660–662, doi:10.1016/j.envsoft.2007.07.004.
- Pickart, R. S., D. J. Torres, and R. A. Clarke (2002), Hydrography of the Labrador Sea during active convection, *J. Phys. Oceanogr.*, *32*, 428–457, doi:10.1175/1520-0485(2002)032<0428:HOTLSD>2.0.CO;2.
- Rattan, S., P. G. Myers, A.-M. Treguier, S. Theetten, A. Biastoch, and C. Böning (2010), Towards an understanding of Labrador Sea salinity drift in eddy-permitting simulations, *Ocean Modell.*, *35*, 77–88, doi:10.1016/j.ocemod.2010.06.007.
- Renfrew, I. A., G. W. K. Moore, P. S. Guest, and K. Bunke (2002), A comparison of surface layer and surface turbulent flux observations over the Labrador Sea with ECMWF analyses and NCEP reanalyses, *J. Phys. Oceanogr.*, *32*, 383–400, doi:10.1175/1520-0485(2002)032<0383:ACOSLA>2.0.CO;2.
- Rykova, T., F. Straneo, J. M. Lilly, and I. Yashayaev (2009), Irminger current anticyclones in the Labrador Sea observed in the hydrographic record, 1990–2004, *J. Mar. Res.*, *67*, 361–384, doi:10.1357/002224009789954739.
- Sandwell, D. T., and W. H. F. Smith (1997), Marine gravity anomaly from Geosat and ERS-1 satellite altimetry, *J. Geophys. Res.*, *102*, 10,039–10,054, doi:10.1029/96JB03223.
- Schott, F. A., R. Zantopp, L. Stramma, M. Dengler, J. Fischer, and M. Wibaux (2004), Circulation and deep-water export at the western exit of the subpolar North Atlantic, *J. Phys. Oceanogr.*, *34*, 817–843, doi:10.1175/1520-0485(2004)034<0817:CADEAT>2.0.CO;2.
- Schott, F. A., L. Stramma, B. S. Giese, and R. Zantopp (2009), Labrador Sea convection and subpolar North Atlantic Deep Water export in the SODA assimilation model, *Deep Sea Res., Part I*, *56*, 926–938, doi:10.1016/j.dsr.2009.01.001.
- Shchepetkin, A. F., and J. C. McWilliams (2003), A method for computing horizontal pressure-gradient force in an oceanic model with a nonaligned vertical coordinate, *J. Geophys. Res.*, *108*(C3), 3090, doi:10.1029/2001JC001047.
- Shchepetkin, A. F., and J. C. McWilliams (2005), The regional oceanic modeling system (ROMS): A split-explicit, free-surface, topography-following-coordinate oceanic model, *Ocean Modell.*, *9*, 347–404, doi:10.1016/j.ocemod.2004.08.002.
- Smith, T. M., and R. W. Reynolds (2004), Improved extended reconstruction SST (1854–1997), *J. Clim.*, *17*, 2466–2477, doi:10.1175/1520-0442(2004)017<2466:IEROS>2.0.CO;2.
- Spall, M. A. (2004), Boundary currents and watermass transformation in Marginal Seas, *J. Phys. Oceanogr.*, *34*, 1197–1213, doi:10.1175/1520-0485(2004)034<1197:BCAWTI>2.0.CO;2.
- Straneo, F. (2006a), Heat and freshwater transport through the central Labrador Sea, *J. Phys. Oceanogr.*, *36*, 606–628, doi:10.1175/JPO2875.1.
- Straneo, F. (2006b), On the connection between dense water formation, overturning, and poleward heat transport in a convective basin, *J. Phys. Oceanogr.*, *36*, 1822–1840, doi:10.1175/JPO2932.1.
- Talley, L. D., and M. S. McCartney (1982), Distribution and circulation of Labrador Sea Water, *J. Phys. Oceanogr.*, *12*, 1189–1205, doi:10.1175/1520-0485(1982)012<1189:DACOLS>2.0.CO;2.
- Thompson, D. W., and J. M. Wallace (1998), The Arctic Oscillation signature in the wintertime geopotential height and temperature fields, *Geophys. Res. Lett.*, *25*, 1297–1300, doi:10.1029/98GL00950.
- Våge, K., R. S. Pickart, V. Thierry, G. Reverdin, C. M. Lee, B. Petrie, T. A. Agnew, A. Wong, and M. H. Ribergaard (2009), Surprising return of deep convection to the subpolar North Atlantic Ocean in winter 2007–2008, *Nat. Geosci.*, *2*, 67–72, doi:10.1038/ngeo382.
- van Aken, H. M., M. F. de Jong, and I. Yashayaev (2011), Decadal and multi-decadal variability of Labrador Sea Water in the north-western North Atlantic Ocean derived from tracer distributions: Heat budget, ventilation, and advection, *Deep Sea Res., Part I*, *58*, 505–523, doi:10.1016/j.dsr.2011.02.008.
- Visbeck, M., E. P. Chassignet, R. Curry, T. Delworth, B. Dickson, and G. Krahnmann (2003), The ocean's response to North Atlantic Oscillation variability, in *The North Atlantic Oscillation: Climatic Significance and Environmental Impact*, *Geophys. Monogr. Ser.*, vol. 134, edited by J. Hurrell et al., pp. 113–145, AGU, Washington, D. C., doi:10.1029/134GM06.
- Warner, J. C., W. R. Geyer, and J. A. Lerczak (2005), Numerical modeling of an estuary: A comprehensive skill assessment, *J. Geophys. Res.*, *110*, C05001, doi:10.1029/2004JC002691.
- Wilkin, J. L. (2006), The summertime heat budget and circulation of south-east New England shelf waters, *J. Phys. Oceanogr.*, *36*, 1997–2011, doi:10.1175/JPO2968.1.
- Wunsch, C., P. Heimbach, R. M. Ponte, I. Fukumori, and the ECCO-GODAE Consortium Members (2009), The global general circulation of the ocean estimated by the ECCO Consortium, *Oceanography*, *22*(2), 88–103, doi:10.5670/oceanog.2009.41.
- Yashayaev, I. (2007), Hydrographic changes in the Labrador Sea, 1960–2005, *Prog. Oceanogr.*, *73*, 242–276, doi:10.1016/j.pocean.2007.04.015.
- Yashayaev, I., and B. J. W. Greenan (2011), Environmental conditions in the Labrador Sea in 2010, *Rep. N5893*, Northwest Atlantic Fish. Org., Sci. Council, Dartmouth, N. S., Canada, June.
- Yashayaev, I., and J. W. Loder (2009), Enhanced production of Labrador Sea Water in 2008, *Geophys. Res. Lett.*, *36*, L01606, doi:10.1029/2008GL036162.
- Yashayaev, I., J. R. N. Lazier, and R. A. Clarke (2003), Temperature and salinity in the central Labrador Sea, in *Hydrobiological Variability in the ICES Area, 1990–1999*, *ICES Mar. Sci. Ser.*, vol. 219, edited by W. Turrell, pp. 32–39, Int. Council for the Explor. of the Sea, Copenhagen.
- Yashayaev, I., H. M. van Aken, N. P. Holliday, and M. Bersch (2007a), Transformation of the Labrador Sea Water in the subpolar North Atlantic, *Geophys. Res. Lett.*, *34*, L22605, doi:10.1029/2007GL031812.
- Yashayaev, I., M. Bersch, and H. M. van Aken (2007b), Spreading of the Labrador Sea Water to the Irminger and Iceland basins, *Geophys. Res. Lett.*, *34*, L10602, doi:10.1029/2006GL028999.
- Zhu, J., E. Demirov, F. Dupont, and D. Wright (2010), Eddy-permitting simulations of the sub-polar North Atlantic: Impact of the model bias on water mass properties and circulation, *Ocean Dyn.*, *60*, 1177–1192, doi:10.1007/s10236-010-0320-4.